

# Breaking the hidden symmetry in the Ginzburg-Landau equation

Arjen Doelman

Mathematisch Instituut, Universiteit Utrecht, P.O. Box 80.010,  
3508 TA Utrecht, the Netherlands

May 30, 1997

## Abstract

In this paper we study localised, traveling, solutions to a Ginzburg-Landau equation to which we have added a small,  $O(\varepsilon)$ ,  $0 < \varepsilon \ll 1$ , quintic term. We consider this term as a model for the higher order nonlinearities which appear in the derivation of the Ginzburg-Landau equation. By a combination of a geometrical approach and an explicit perturbation analysis we are able to relate the family of Bekki & Nozaki solutions of the cubic equation [1] to a curve of co-dimension 2 homoclinic bifurcations in parameter space. Thus, we are able to interpret the hidden symmetry – which has been conjectured to explain the existence of the Bekki & Nozaki solutions – from the point of view of bifurcation theory. We show that the quintic term breaks this hidden symmetry and that the one-parameter family of Bekki & Nozaki solutions is embedded in a two-parameter family of homoclinic solutions which exist at a co-dimension 1 homoclinic bifurcation. Furthermore, we show, mainly by geometrical arguments, that the addition of the small quintic term can create large families of traveling localised structures that cannot exist in the cubic case. These solutions exist in open subsets of the parameter space and correspond to structurally stable multi- or  $N$ -circuit heteroclinic orbits in an ODE reduction and have a monotonically decreasing/increasing amplitude, except for a number,  $N$ , of (relatively fast) ‘jumps’.

*Keywords:* nonlinear stability, modulation equations, singularly perturbed ODE, homoclinic bifurcations, heteroclinic orbits.

*Mathematics subjects classification:* 34C23, 34C37, 34E15, 35Q35, 76E30.

# 1 Introduction

The (cubic) Ginzburg-Landau equation governs the nonlinear evolution of perturbations of a ‘simple’ solution of a basic system of partial differential equations (in an unbounded domain) at near-critical conditions, provided that this basic system satisfies some generic conditions (see for instance [11]) Therefore, this equation appears in many fields of science. The asymptotic validity of the Ginzburg-Landau equation has been proved for large classes of systems (see for instance [4], [14] and [3] for a review). However, the Ginzburg-Landau equation is the product of an asymptotic expansion: the equation with only cubic terms is only the  $O(1)$  part of a more extended equation (see for instance [12], [7]). In this paper we will investigate the influence of these higher order terms on the behaviour of the traveling solutions of the equation. As in [26], [27] and [30] we therefore consider an extended Ginzburg-Landau equation of the following type:

$$(1.1) \quad u_t = ru + \alpha u_{xx} + \beta |u|^2 u + \varepsilon \gamma |u|^4 u,$$

where  $r \in \mathbf{R}$  corresponds to the bifurcation/control parameter in the original system and  $\alpha, \beta \in \mathbf{C}$ ;  $\alpha$  and  $\beta$  can be computed explicitly from the underlying system ([11]). The higher order nonlinear effects are modeled by the quintic term  $\varepsilon \gamma |u|^4 u$  where  $|\varepsilon| \ll 1$  and  $\gamma \in \mathbf{C}$ . We emphasize here that in general one cannot derive an equation like (1.1) from a ‘generic’ basic system: although the quintic terms will appear as higher order corrections to the cubic equation, we ignore here other higher order terms of the same, or of an even a larger – but still  $o(1)$  – magnitude, such as  $u_{xxx}$ ,  $|u|^2 u_x$ ,  $u^2 \bar{u}_x$  ([12], [7]). However, as in [26], [27], [30], we consider (1.1) as a suitable *model* by which we can study the influence of the small, nonlinear higher order effects. Moreover, quintic equations like (1.1) have been the subject of many studies. For instance, the quintic Ginzburg-Landau equation has been analysed as a model to explain the behaviour of traveling patterns in binary fluid convection (see, for instance, [2] for experimental observations and [29] for references on the analysis.).

In this paper we will restrict ourselves to the analysis of traveling waves to (1.1) of the type

$$u(x, t) = U(\xi) e^{i\omega t}, \quad \text{where } \xi = x + vt.$$

Thus, we reduce the partial differential equation to a three-dimensional set of ordinary differential equations with two free parameters  $v$  and  $w$  (see section 2). Furthermore, we will mainly focus on the existence of so-called localised, or coherent, structures. These are solutions to (1.1) which approach a simple periodic solution of the type  $u(x, t) = R e^{i(\kappa x + \omega t)}$  as  $x \rightarrow \pm\infty$  and therefore correspond to heteroclinic or homoclinic solutions in the ODE reduction. Moreover, we only consider localised structures which connect stable, non-zero periodic patterns at  $\pm\infty$  (see subsection 2.3). These types of solutions have been, and still are, the subject of both physical and mathematical research since they correspond to patterns which have been observed in experiments (see for instance [2]) and in numerical simulations (see [29] for an overview). Moreover, the mathematical analysis of the existence and the stability of these solutions is closely connected to the development of mathematical theories (see for instance [23], [17], [18], [9], [8]).

A central role will be played by the so-called hidden, or inner, symmetry which has been conjectured to exist in the cubic Ginzburg-Landau equation (see [29], [26], [27], [30]). This conjecture is based on the existence of a one-parameter family of solutions to the cubic Ginzburg-Landau equation, the Bekki & Nozaki solutions [1]. Bekki and Nozaki constructed explicit solutions of the form

$$(1.2) \quad u(x, t) = [e^{i\frac{1}{2}q\xi} F(\xi)G(\xi)^{-(1+i\lambda)}]e^{iwt}, \quad \xi = x + vt,$$

where  $F(\xi) = \mu(e^{k\xi} + ze^{-k\xi})$  and  $G(\xi) = e^{k\xi} + e^{-k\xi}$ . Inserting this expression into (1.1) (with  $\varepsilon = 0$ ) yields a (nonlinear) system of 8 equations for the 8 (real) parameters  $v$ ,  $w$ ,  $q$ ,  $\lambda$ ,  $\mu$ ,  $k$  and  $z = z_r + iz_i$ . However, if one solves this system ‘a miracle happens’ (see [1], [29], [6]): one of these equations turns out to be redundant. Thus, one finds a one-parameter family of traveling, localised solutions to the cubic Ginzburg-Landau equation. Moreover, these solutions correspond to a one-parameter family of connections between one-dimensional stable and one-dimensional unstable manifolds of critical points in the three-dimensional ODE reduction ([29], [6]). This yields that the Bekki & Nozaki solutions violate a simple geometrical counting argument [29]: a connection between two one-dimensional manifolds in a three-dimensional space can generically only exist for discrete values of the free parameters  $v$  and  $w$ . The existence of a ‘hidden’ symmetry was conjectured to explain the family of Bekki & Nozaki solutions. Moreover, we quote from the paper by van Saarloos and Hohenberg ([29], page 339): ”The existence of a family of sources (= the Bekki & Nozaki solutions) in our view presents a serious challenge to our understanding of phase space methods (= the ODE reduction) as applied to coherent structures (= localised solutions)”.

One of the main results of this paper is that the phase space methods/ODE reduction is a very suitable ‘tool’ to understand the hidden symmetry. By studying the ODE reduction of (1.1) in the context of bifurcation analysis, the hidden symmetry can be identified as being related to a co-dimension 2 homoclinic (that is: non-local) bifurcation. The main idea behind this interpretation can be explained as follows. By a number of (re)scalings one can reduce the number of parameters in the ODE reduction of (1.1) to (essentially) three,  $V$ ,  $W$  and  $P$  (sections 2 and 3). Parameter  $P$  corresponds to the quintic extension:  $P = 0$  describes the cubic case. Thus, one can perform a bifurcation analysis in the three-dimensional  $(V, W, P)$ -parameter space: a co-dimension 1 bifurcation, such as a (local) saddle node bifurcation, corresponds to a surface,  $\mathcal{C}_{sn}$ , in this space at which such a bifurcation occurs. Since we restrict ourselves to equations of the type (1.1) which are ‘near’ an integrable limit (that is either the real Ginzburg-Landau limit or the nonlinear Schrödinger limit, see section 2), we can explicitly show in section 3 that there is a close relation between the creation/annihilation of structurally stable heteroclinic orbits and the creation/annihilation of periodic solutions of the ODE by a homoclinic bifurcation (see also [8]). Furthermore, we are able to determine the surface  $\mathcal{C}_h$  of such co-dimension 1 homoclinic bifurcations explicitly by approximating a certain Poincaré map (see section 3). Generically one expects that the two surfaces  $\mathcal{C}_{sn}$  and  $\mathcal{C}_h$  intersect along a curve of co-dimension 2 ‘homoclinic/saddle node’ bifurcations. In section 4 we show that outside this curve the periodic solutions and the heteroclinic solutions merge in a homoclinic solution at the bifurcation on  $\mathcal{C}_h$ . This homoclinic solution is a connection between a two-dimensional stable/unstable manifold and a one dimensional unstable/stable manifold (see

Figure 3). At the co-dimension 2 curve  $\mathcal{C}_{sn} \cap \mathcal{C}_h$ , the homoclinic orbit is replaced by a heteroclinic orbit, which is the connection between two one-dimensional stable/unstable manifolds (Figure 3). From a bifurcation theory point of view this is a very natural phenomenon which can, for instance, be studied by the geometrical methods developed in [8] (see section 4). Moreover, by the explicit expressions derived in section 3 we find that  $\mathcal{C}_{sn} \cap \mathcal{C}_h$  consists of three branches, one of them is a curve in the  $\{P = 0\}$ -plane, which corresponds to the cubic Ginzburg-Landau case. The strength of the geometrical interpretation combined with the explicit perturbation analysis is that we can show in section 4 that the  $\{P = 0\}$ -branch of the curve  $\mathcal{C}_{sn} \cap \mathcal{C}_h$  corresponds directly to the family of Bekki & Nozaki solutions (1.2) which ‘caused’ the hidden symmetry. The other two branches correspond to degenerate cases (for instance for parameter combinations such that there is a simple, explicit symmetry present in the ODE reduction, see subsection 4.1)

Thus, the existence of the Bekki & Nozaki family can be understood in a very natural way: by the geometrical arguments we know that there must be a one-parameter curve of heteroclinic connections between two one dimensional stable/unstable manifolds in the three dimensional parameter space, related to the curve  $\mathcal{C}_{sn} \cap \mathcal{C}_h$ . Note however, that although the geometrical interpretation enables us to study the Bekki & Nozaki solutions (1.2) and their response to the perturbation  $P \neq 0$ , it does not tell us why (a branch of) the curve  $\mathcal{C}_{sn} \cap \mathcal{C}_h$  can be found exactly in the  $\{P = 0\}$ -plane. Thus, the geometrical approach does not explain the hidden symmetry in the cubic Ginzburg-Landau equation, but it does enables us to study it in detail. Moreover, by considering  $P \neq 0$  we can ‘break’ the hidden symmetry and consider the impact of the small quintic term in (1.1) within the geometrical framework. As a consequence, we – for instance – are able (unlike in [26], [27], [30]) to embed the one-parameter family of Bekki & Nozaki solutions (1.2) into a two parameter family of homoclinic solutions (of the above described type): for every value of  $P$  – and thus every  $\gamma$  in (1.1) – there exists a one parameter family of homoclinic solutions in (wave speed  $v$ , frequency  $w$ )-space; this family merges with the Bekki & Nozaki heteroclinic orbits (1.2) in the limit  $P \rightarrow 0$  (in fact, it is a little bit more subtle: a homoclinic solution merges with a heteroclinic cycle formed by the Bekki & Nozaki solution and a part of a so-called slow manifold (see below, section 4 and Theorem 5.1).

The fact that we realise that the heteroclinic and homoclinic solutions – and thus the localised structures – must be intersections of the two-dimensional stable and unstable manifolds,  $W^s(\cdot)$  and  $W^u(\cdot)$ , of a certain slow manifold  $\Sigma$ , can be considered as the backbone of the geometrical approach (section 3 and 4). This slow manifold must exist since we study the ODE reductions near an integrable limit which possesses a family of homoclinic orbits (section 3, [13], [33]). This interpretation allows us to prove the existence of large families of multi-circuit heteroclinic orbits which so far has not been noted in the literature.

The existence of these orbits follows from a theorem which was already proved in [8] for a – fairly simple – model problem. In section 4 we prove an equivalent of the theorem in [8] which is valid for the ODE reduction derived from (1.1) – near an integrable limit. We show in subsection 4.2 that  $W^s(\cdot)$  and  $W^u(\cdot)$  can intersect in two essentially different ways. If there exist two critical points  $S$  and  $\hat{S}$  on  $\Sigma$ , and if their position is ‘correct’ – see subsection 4.2 – with respect to this intersection, there will be so-called a structurally

stable 1-circuit heteroclinic connection  $\in W^s(\cdot) \cap W^u(\cdot)$  between  $S$  and  $\hat{S}$  in both cases. However, in the first case, (A), there cannot be any other higher order intersections, while in the second case, (B), it is shown that there exist countably infinitely many higher order intersections of  $W^s(\cdot)$  and  $W^u(\cdot)$ . These intersections correspond to so-called multi- or  $N$ -circuit heteroclinic orbits between  $S$  and  $\hat{S}$  which are (also) structurally stable. Thus, these connections exist for open regions in the parameter space. In the context of the PDE (1.1), these solutions are localised structures connecting two different stable periodic ‘patterns’ at  $x = \pm\infty$  in a monotonic way (that is,  $|u|$  increases/decreases monotonically) except for a number,  $N$  (the same  $N$ ), of ‘holes’ or ‘jumps’ where  $|u|$  changes rapidly (see subsection 5.2).

In section 5 we show (Theorems 5.2 and 5.3) that both types of heteroclinic solutions exists in (1.1) – near an integrable limit – for open regions in the  $(V, W, P)$ -parameter space. However, as was already noted in [8]: the cubic Ginzburg-Landau equation only has structurally stable heteroclinic solutions of the case (A) type (see subsection 5.2, Figure 5). Thus, there are no ‘multi-jump’ solutions of the above described type. The type (B) multi-circuit heteroclinic orbits exist in Ginzburg-Landau equations to which the small quintic term  $\varepsilon\gamma|u|^4u$  has been added, where  $\gamma$  is such that  $P \in (-\frac{15}{11} + O(\varepsilon), -\frac{1}{2} + O(\varepsilon))$  (Theorem 5.3).

We conclude that the influence of the higher order nonlinearities modeled by the quintic terms in (1.1) can not be neglected, no matter how small one chooses  $\varepsilon$ : due to the higher order nonlinearities there exist localised solutions to (1.1) of the above described ‘multi-jump’ type which cannot exist in the cubic equation. Moreover, these solutions are not  $O(\varepsilon)$  close to solutions of the cubic equation (for all  $x, t$ ). Furthermore we conclude that the geometrical approach of this paper – in combination with explicit perturbation analysis – enables us to handle the hidden symmetry – or better: the Bekki & Nozaki solutions – in the cubic Ginzburg-Landau equation and interpret it in terms of bifurcation theory.

**Remark 1.1** The structure of this paper is as follows: in section 2 we first derive two ODE reductions, one near the real Ginzburg-Landau integrable limit, the other near the nonlinear Schrödinger limit. By scaling we reduce the amount of parameters considerably and find that both integrable limits are in essence the same (in the ODE context). In subsection 2.2 we mention some important properties of the integrable system which we will use frequently. In subsection 2.3 we study the critical points of these systems, thereby deriving the first two bifurcation manifolds in  $(V, W, P)$ -space,  $\mathcal{C}_{sn}$  and  $\mathcal{C}_d$ . In subsection 3.1 we construct the approximation of a Poincaré map by which we can study the existence of periodic solutions. Thus we are able to determine an explicit expression of the homoclinic bifurcation manifold  $\mathcal{C}_h$ . In subsection 3.2 we introduce the slow manifold, and its stable and unstable manifolds  $W^s(\cdot)$  and  $W^u(\cdot)$ . We determine an explicit expression for the first intersections of  $W^s(\cdot)$  and  $W^u(\cdot)$ . Based on this expression we determine a fourth bifurcation manifold  $\mathcal{C}_t$ . In section 4 we present the geometric interpretation of the hidden symmetry described above. We also discuss the degenerate, symmetrical, case  $V = 0$ . Furthermore we formulate and prove the theorem described above which enables us to distinguish between heteroclinic connections of type (A) and (multi-circuit) orbits

of type (B). Section 5 can be seen as the combination of 3 and 4: here we combine the explicit analytical results of section 3 with the geometrical approach of section 4. As a consequence we are able to formulate and prove the above mentioned Theorems 5.1, 5.2 and 5.3. In section 6 we discuss some aspects of the relation of the results of this paper with the literature.

**Remark 1.2** In this paper we do not pay any attention to the large – that is  $O(\frac{1}{\sqrt{\varepsilon}})$  – solutions introduced by the quintic term of  $O(\varepsilon)$  in (1.1). These solutions are inconsistent with the assumptions on which the derivation of the Ginzburg-Landau equation is based (see [12], [7]).

## 2 The ODE reductions

### 2.1 The derivation

There are two different integrable limits to (1.1): the real Ginzburg-Landau equation ( $\text{Im}\alpha = \text{Im}\beta = \varepsilon = 0$ ) – the stationary problem is integrable – and the nonlinear Schrödinger equation ( $r = \text{Re}\alpha = \text{Re}\beta = \varepsilon = 0$ ). The first case appears generically when the underlying system is reflection symmetric, see [6] for a list of physical problems – such as convection problems – in which the (nearly) real Ginzburg-Landau equation occurs naturally. The second case can not be connected that easily to a property of the underlying system. In fact, the limit  $\text{Re}\alpha \rightarrow 0$  is degenerate from the derivational point of view:  $\text{Re}\alpha = 0$  corresponds to a linearized stability problem in the underlying system with a neutral curve that has a degenerate (that is non-quadratic) minimum [11]. Moreover, it has been shown in [12] and [7] that the cubic Ginzburg-Landau equation must be extended in the case  $\text{Re}\beta$  ‘small’. Thus, the nonlinear Schrödinger limit is not a very natural limit if one considers the Ginzburg-Landau equation only as a modulation equation. However, near the nonlinear Schrödinger limit one can consider (1.1) as a natural perturbation (see also [30]). Note that – by rescaling – one can also obtain the nonlinear Schrödinger equation from (1.1) by taking the limit  $\text{Im}\alpha, \text{Im}\beta \rightarrow \infty$ .

By scaling we can write (1.1) near the real Ginzburg-Landau (RGL) limit as

$$(2.1) \quad u_t = u + (1 + i\varepsilon a)u_{xx} - (1 + i\varepsilon b)|u|^2u + \varepsilon(p + iq)|u|^4u,$$

where we made the classical assumptions  $r > 0$  and  $\text{Re}\beta < 0$ ; near the nonlinear Schrödinger (NLS) limit (1.1) can be scaled into

$$(2.2) \quad u_t = \varepsilon r u + (\pm i + \varepsilon a)u_{xx} + (\pm i + \varepsilon b)|u|^2u + \varepsilon(p + iq)|u|^4u.$$

As yet, we do not choose the signs of  $\text{Im}\alpha$  and  $\text{Im}\beta$  in (2.2). Note that we assume in both cases that all perturbations are of the same order ( $O(\varepsilon)$ ) as the quintic term. Next we start to look for traveling waves and set

$$(2.3) \quad u(x, t) = U(x + vt)e^{iwt}.$$

In contrast with the parameters in (2.1) and (2.2) – which should be considered as given by the physics of the underlying system – wave speed  $v$  and frequency  $w$  are ‘free’ parameters.

It can be shown [6] that near the RGL limit one must consider  $v = \varepsilon \hat{v}$  and  $w = \varepsilon \hat{w}$  (since the traveling waves can be considered as being bifurcated from the unstable periodic solutions of (2.1)). In the NLS case we do not make  $w = O(\varepsilon)$ , in order to introduce a  $O(1)$  linear term in the equation for  $U$ . However, we do take  $v = \varepsilon \hat{v}$  (see remark 2.1). Due to the phase invariance of solutions to (1.1) it is natural to write  $U$  in polar coordinates

$$(2.4) \quad U(\xi) = \rho(\xi)e^{\theta(\xi)} \quad \text{where } \xi = x + \varepsilon \hat{v}t.$$

We substitute (2.3) and (2.4) into (2.1) and (2.2) and note that  $\Omega = \rho^2 \theta_\xi$  is an integral of the  $\varepsilon \rightarrow 0$  limit in both cases: both systems yield a three-dimensional ODE in  $\rho$ ,  $\sigma = \rho_\xi$  and  $\Omega$ . Near the RGL limit this system is given by

$$(2.5) \quad \begin{cases} \rho_\xi = \sigma \\ \sigma_\xi = -\rho + \rho^3 + \frac{\Omega^2}{\rho^3} + \varepsilon[\hat{v}\sigma - p\rho^5] + O(\varepsilon^2) \\ \Omega_\xi = \varepsilon[(\hat{w} + a)\rho^2 + (b - a)\rho^4 + \hat{v}\Omega - q\rho^6] + O(\varepsilon^2) \end{cases}$$

In the NLS limit we have to be a bit more careful: for  $\varepsilon = 0$  the equation for  $\rho$  reads:

$$\pm(\rho_{\xi\xi} - \frac{\Omega^2}{\rho^3}) - wU \pm |U|^2U = 0.$$

Thus, the integrable limit in the NLS case is (topologically) the same as the integrable limit in the RGL case (that is  $\varepsilon = 0$  in (2.5)) if  $\text{Im}\alpha\text{Im}\beta < 0$  (and one chooses the sign of the free parameter  $w$  correctly). All other combinations of  $\text{sign}(\text{Im}\alpha)$ ,  $\text{sign}(\text{Im}\beta)$  and  $\text{sign}(w)$  correspond to rather trivial unperturbed flows. Since changing the signs of both  $\text{Im}\alpha$  and  $\text{Im}\beta$  is the same as reversing time in the NLS equation we assume from now on that  $\text{Im}\alpha > 0$ ,  $\text{Im}\beta < 0$  and  $w < 0$  (in the NLS case). Thus, we consider exactly the same limit – the defocusing nonlinear Schrödinger equation – as in [30]. The equation for traveling waves near the NLS limit reads:

$$(2.6) \quad \begin{cases} \rho_\xi = \sigma \\ \sigma_\xi = w\rho + \rho^3 + \frac{\Omega^2}{\rho^3} + \varepsilon[\hat{v}\frac{\Omega}{\rho} - q\rho^5] + O(\varepsilon^2) \\ \Omega_\xi = \varepsilon[(aw + r)\rho^2 + (a + b)\rho^4 - \hat{v}\rho\sigma + p\rho^6] + O(\varepsilon^2) \end{cases}$$

Since we are only interested in the leading order effects of the perturbations, we do not pay attention to the  $O(\varepsilon^2)$  terms in (2.5) and (2.6). Thus, we neglect the  $O(\varepsilon^2)$  terms in the sequel. By rescaling we can reduce the amount of parameters in (2.5) and (2.6) considerably. Introducing  $x$ ,  $y$ ,  $z$  and  $t$  instead of  $\rho$ ,  $\sigma$ ,  $\Omega$  and  $\xi$  we find in the RGL case:

$$(2.7) \quad \begin{cases} \dot{x} = y \\ \dot{y} = -x + x^3 + \frac{z^2}{x^3} + \hat{\varepsilon}[Vy + Qx^5] \\ \dot{z} = \hat{\varepsilon}[Wx^2 + x^4 + Px^6 + Vz] \end{cases}$$

where

$$\hat{\varepsilon} = (b - a)\varepsilon, \quad V = \frac{\hat{v}}{b - a}, \quad W = \frac{\hat{w} + a}{b - a}, \quad P = -\frac{q}{b - a}, \quad Q = -\frac{p}{b - a}.$$

In the NLS limit we find:

$$(2.8) \quad \begin{cases} \dot{x} = y \\ \dot{y} = -x + x^3 + \frac{z^2}{x^3} + \hat{\varepsilon}[V\frac{z}{x} + Qx^5] \\ \dot{z} = \hat{\varepsilon}[Wx^2 + x^4 + Px^6 - Vxy] \end{cases}$$

with

$$\hat{\varepsilon} = (a + b)\varepsilon, \quad V = \frac{\hat{v}}{(a + b)\sqrt{-w}}, \quad W = -\frac{r + aw}{w(a + b)}, \quad P = -\frac{pw}{a + b}, \quad Q = \frac{qw}{a + b}.$$

Thus, in both systems there are only four parameters left: the free parameters  $V$  and  $W$  and the parameters  $P$  and  $Q$  which originate from the quintic term in (1.1). Of course we choose the rescalings in order to obtain as much similarity as possible between the systems (2.7) and (2.8). In the sequel we drop the ‘hats’ on the  $\varepsilon$ ’s.

Notice that (2.7) and (2.8) are exactly the same for  $V = 0$ , thus, the stationary problems – that is  $v = 0$  in (2.3) – are essentially the same in (2.1) and (2.2)! Moreover, we will find in section 3 that the parameter  $V$  has a negligible influence on the dynamics in the NLS limit. Therefore, we will mainly study (2.7) in this paper: the NLS case can be obtained from this analysis by taking  $V = 0$  in (2.7). However, the systems (2.7) and (2.8) become invariant under the symmetry  $t \rightarrow -t, x \rightarrow x, y \rightarrow -y, z \rightarrow -z$  when  $V = 0$ . See (the end of) subsection 4.1 for a brief discussion of the additional phenomena created by this symmetry.

**Remark 2.1** The fact that  $V$  can be neglected in (2.8) is not so surprising if one realises that  $v$  does not give rise to non-integrable effects in the NLS limit: if one allows for waves moving with an  $O(1)$  speed in (2.2) with  $\varepsilon = 0$  one finds that the equation for  $U$  is still integrable. However, the integrals of this system are less easy to handle than the integrals of (2.7) and (2.8) for  $\varepsilon = 0$ . Since being able to control the behaviour of these integrals is essential to understanding the dynamics of the perturbed systems we do not consider the case  $v = O(1)$  in the NLS limit in this paper.

Parameter  $Q$  has also no ‘non-integrable’ influence on the flows of (2.7) and (2.8): the term ‘ $\varepsilon Q x^5$ ’ can be added to the second integral  $I$  (2.10). Therefore, we will find that  $Q$  also does not play a role in the following sections.

**Remark 2.2** We do not pay attention to the cases  $a - b = 0$  in (2.1) or  $a + b = 0$  in (2.2) in this paper. Above it is suggested that these cases are singular, but that’s not the case. The singularities are caused by the rescalings, one just has to choose other scalings and then one will derive equations very similar to (2.7) and (2.8).

## 2.2 The integrable limit

The unperturbed system,

$$(2.9) \quad \ddot{x} + x - x^3 - \frac{z^2}{x^3}, \quad \dot{z} = 0,$$

has two integrals,  $z$  and

$$(2.10) \quad I = x^2 + y^2 - \frac{1}{2}x^4 + \frac{z^2}{x^2}.$$

For  $0 < |z_0| < \sqrt{\frac{4}{27}}$  the system has a center and a saddle point in the  $\{z = z_0\}$ -plane. There is a homoclinic solution to the saddle point which is the limit of the family of



periodic solutions encircling the center point. In Figure 1 we show the bounded region in the phase space for which the solutions remain bounded for all  $t$ . Note that these solutions remain bounded away from the singularity at  $x = 0$  for  $z \neq 0$ . We define  $E$ , the (bounded) region in the  $(I, z)$ -plane for which the solutions are bounded, by its boundary  $\partial E$ :

$$(2.11) \quad \partial E = \{(I, z) : z^2 = X^2 - X^3, I = 2X - \frac{3}{2}X^2, X \in [0, 1]\}.$$

Note that  $X$  corresponds to the square of the  $x$ -coordinate of the critical points: for  $0 < X < \frac{2}{3}$   $\partial E$  is given by the center points,  $\frac{2}{3} < X < 1$  describes the saddle point/homoclinic orbit part of  $\partial E$ ;  $X = \frac{2}{3}$  corresponds to the saddle-center bifurcation at  $z = \sqrt{\frac{4}{27}}$  (Figure 1). At  $z = 0$  the system degenerates: solutions pass through the  $\{x = 0\}$  axis (recall that  $x$  corresponds to  $\rho = |u|$  (see also [5])). In this paper we will (try to) avoid both degenerations – at  $z = 0$  and  $z = \sqrt{\frac{4}{27}}$ .

We now present some technical properties of system (2.9) which we will use in the next sections. Especially in section 3 we will frequently use the periods of the solutions to (2.9):

$$(2.12) \quad T_i(I, z) = \oint \frac{X^i}{\sqrt{\frac{1}{2}X^3 - X^2 + IX - z^2}} dX, \quad i = 1, 2, \dots$$

where the (complex) contour is taken around the bounded interval on which the denominator of the integrand is defined. Note that  $T_0(I, z)$  is the period of a periodic solution (for  $(I, z) \in E$ ). All higher periods can be expressed in  $T_0$  and  $T_1$ :

$$(2.13) \quad T_2 = \frac{4}{3}T_1 - \frac{2}{3}IT_0, \quad T_3 = \frac{2}{5}\left(\frac{16}{3} - 3I\right)T_1 + \frac{4}{5}\left(z^2 - \frac{4}{3}I\right)T_0, \quad \text{etc.}$$

These formulae can be obtained by evaluating the expressions

$$0 = \oint \frac{d}{dX} (X^j \sqrt{\frac{1}{2}X^3 - X^2 + IX - z^2}) dX, \quad j = 1, 2, \dots$$

(see [6] for more details). As a consequence, it is useful to introduce

$$(2.14) \quad \mathcal{T}(I, z) = \frac{T_i(I, z)}{T_0(I, z)}.$$

Both  $T_1$  and  $T_0$  diverge as  $I \rightarrow I_s$ , where  $I_s$  is the value of  $I$  at the unperturbed homoclinic orbit (see (2.11)). However, it is easy to verify that  $\mathcal{T} \rightarrow X_s(z)$ , the square of the  $x$ -coordinate of the saddle point, as  $I \rightarrow I_s$ . In [6] it is shown that  $\mathcal{T}(I, z)$  is a monotonously increasing function of  $I$  for given  $z$  in the interval  $(-\sqrt{\frac{4}{27}}, \sqrt{\frac{4}{27}})$ . Since we will mainly use  $\mathcal{T}(I, z)$  for  $I$  near  $I_s$  the following approximation will be useful:

$$(2.15) \quad \mathcal{T}(I_s - \delta, z) = X_s - \frac{1}{4(3X_s - 2)|\log \delta|} + \text{h.o.t. for } 0 < \delta \ll 1,$$

where  $X_s = X_s(z) \in (\frac{2}{3}, 1)$ . We (again) refer to [6] for the derivation.

We will also need explicit formulae for the homoclinic solutions in (2.9). Although we know that these solutions are Bekki & Nozaki solutions (1.2) – see [6] – we prefer another

description which can be obtained directly from (2.9) by introducing  $X = x^2$  (and using (2.10):

$$\ddot{X} - 2I + 4X - 3X^2 = 0.$$

This equation has solutions of the type  $A + B \tanh^2(\lambda t)$  if  $I = I_s$ . We find, by parametrizing by  $X_s = X_s(z)$  (see (2.11):

$$(2.16) \quad x_h(t; z) = [2(1 - X_s) + (3X_s - 2) \tanh^2(\frac{1}{2}\sqrt{2}(3X_s - 2)t)]^{\frac{1}{2}}, \quad X_s \in (\frac{2}{3}, 1).$$

### 2.3 Critical points

The critical points to (2.7) and (2.8) correspond to ‘harmonic’ periodic solutions of the type  $u(x, t) = R e^{i(\kappa x + \omega t)}$  of (2.1) and (2.2). The stability of these solutions to the unperturbed Ginzburg-Landau equation is well-known (see for instance [31], [25]). In the limit  $\varepsilon \rightarrow 0$  one finds that the solutions to (2.1) or (2.2) that correspond to the center points of (2.9) are unstable and that the saddles are stable. The degenerate points at  $z = \pm\sqrt{\frac{4}{27}}$  correspond to the so-called Eckhaus stability boundary [10]. One can distinguish between three different types of critical points to (2.7) and (2.8): perturbed saddle points, perturbed center points and points which are  $O(\varepsilon)$  close to the degenerate point at  $z = \pm\sqrt{\frac{4}{27}}$ . It is a straightforward job to check that the ‘saddles’ are stable and that the ‘centers’ are unstable as solutions of (2.1) or (2.2). In this paper we focus on connections between these perturbed saddles and neglect the other critical points. In the context of the modulation equations this means that we search for traveling ‘localised’ structures which connect stable patterns at  $x \rightarrow \pm\infty$ .

The critical points are determined (up to  $O(\varepsilon)$ ) by

$$(2.17) \quad z^2 = x^4(1 - x^2) \quad \text{and} \quad Wx^2 + x^4 + Px^6 + Vz = 0$$

in the RGL case; the NLS system yields the same equations with  $V = 0$  (thus,  $V$  has no  $O(1)$  influence on the critical points). There are two curves  $-\mathcal{C}_{sn} = \mathcal{C}_{sn}(P)$  and  $\mathcal{C}_d = \mathcal{C}_d(P)$  – in the  $(V, W)$ -plane which decide about the number of perturbed saddle points for a given parameter combination: at  $\mathcal{C}_{sn}$  two (perturbed) saddles merge in a saddle node bifurcation and at  $\mathcal{C}_d$  the  $x$ -coordinate of the saddle point becomes  $\sqrt{\frac{2}{3}}$ : the perturbed saddle approaches the degeneration at  $z = \pm\sqrt{\frac{4}{27}}$ . These curves can be computed explicitly:

$$(2.18) \quad \mathcal{C}_{sn} = \{(V, W) = (V_{sn}(X), W_{sn}(X)), \quad X = X_s \in (\frac{2}{3}, 1)\} \quad \text{where} \\ V_{sn}(X) = \pm 2(1 + 2PX)\sqrt{1 - X}, \quad W_{sn}(X) = -2 + X - PX(4 - 3X);$$

the  $\pm$  corresponds to  $z = \pm X\sqrt{1 - X}$  (with  $X = x^2$ , see (2.11));

$$(2.19) \quad \mathcal{C}_d = \{(V, W) : V^2 = \frac{1}{27}(9W + 6 + 4P)^2\}.$$

The curve  $\mathcal{C}_{sn}$  is tangent to  $\mathcal{C}_d$  as  $X \rightarrow \frac{2}{3}$ . In section 5 we will study these, and other, curves in more detail.

Note that all perturbed saddle points are on the slow manifold, which exists  $O(\varepsilon)$  near the curve of saddle points to the unperturbed system (see subsection 3.2, [13], [33]). The direction of the flow on, is determined by  $\dot{z}$  and thus by the weak ( $O(\varepsilon)$ ) eigenvalues of the perturbed saddles. The slow manifold, is not influenced by the degeneration at  $z = 0$ .

### 3 Perturbation analysis

#### 3.1 The approximation of a Poincaré map

Since we are only interested in solutions which remain bounded for  $t \rightarrow \pm\infty$  – recall that  $t$  corresponds to the moving coordinate  $\xi = x + vt$  in (1.1) – we only study solutions of the perturbed problems with values of the integrals  $I$  and  $z$  in an  $O(\varepsilon)$  neighbourhood of  $E$  (see (2.11). In this region the flow is dominated by the periodic orbits of the unperturbed system, thus it is natural to ‘average’ this effect by constructing a return map  $\mathcal{P}$ ,

$$\mathcal{P}(I, z) \stackrel{\text{def}}{=} (I + \Delta I(I, z), z + \Delta z(I, z)),$$

where

$$\Delta I(I, z) = \int_0^{T_\varepsilon(I, z)} \dot{I}(\gamma_\varepsilon(t)) dt, \quad \Delta z(I, z) = \int_0^{T_\varepsilon(I, z)} \dot{z}(\gamma_\varepsilon(t)) dt$$

and  $\gamma_\varepsilon(t) = (x_\varepsilon(t), y_\varepsilon(t), z_\varepsilon(t))$  is a solution of (2.7) or (2.8) with  $y_\varepsilon(0) = 0, z_\varepsilon(0) = z$  and  $x_\varepsilon(0)$  such that  $I(0) = I$  and  $0 < x_\varepsilon(0) < x_c$  ( $x_c = x_c(z)$  is the  $x$ -coordinate of the unperturbed center points);  $T_\varepsilon(I, z)$  is the return time (and is  $O(\varepsilon)$  close to  $T_0(I, z)$  as long as  $\gamma_\varepsilon$  is not too close to the unperturbed homoclinic orbits). We can now approximate  $\gamma_\varepsilon(t)$  by the solution of (2.9) with the same initial conditions. This causes an  $O(\varepsilon^2)$  error since both  $\dot{I}$  and  $\dot{z}$  are  $O(\varepsilon)$ :

$$\begin{aligned} \Delta I(I, z) &= \int_0^{T_0(I, z)} \dot{I}((x_0(t), y_0(t), z)) dt + O(\varepsilon^2) \\ \Delta z(I, z) &= \int_0^{T_0(I, z)} \dot{z}((x_0(t), y_0(t), z)) dt + O(\varepsilon^2). \end{aligned}$$

By (2.10) we can compute  $\dot{I}$  and change variables (introducing  $X = x^2$ ). We find in the RGL case:

$$(3.1) \quad \Delta_{\text{rgl}} I(z, I) = \varepsilon \oint \frac{(IV + zW) + (z - V)X + (\frac{1}{2}V + zP)X^2}{\sqrt{\frac{1}{2}X^3 - X^2 + IX - z^2}} dX + O(\varepsilon^2)$$

where the contour integral is taken around the interval  $[X_l(I, z), X_r(I, z)]$ ;  $\sqrt{X_l}$  and  $\sqrt{X_r}$  are the  $x$ -coordinates of the intersections of the orbit  $(x_0(t), y_0(t))$  with the  $y$ -axis. Using (2.12) and (2.13) we can write (3.1) as

$$(3.2) \quad \frac{\Delta_{\text{rgl}} I(z, I)}{\varepsilon} = \frac{1}{3}(-V + 3z + 4Pz)T_1(I, z) + \frac{1}{3}(2IV - 2IPz + 3Wz)T_0(I, z) + O(\varepsilon).$$

Note that the parameter  $Q$  does not appear in (3.2): its influence has been ‘averaged out’. Analogously we find, at leading order

$$(3.3) \quad \frac{\Delta_{rglz}(z, I)}{\varepsilon} = \frac{1}{30}[(20 + (32 - 18I)P + 15W)T_1 - (10I + 16IP - 15Vz - 12Pz^2)T_0].$$

If we perform the same calculations for the NLS limit we see that all terms involving the parameters  $V$  and  $Q$  disappear by averaging, thus we conclude

$$(3.4) \quad \Delta_{nls}I(z, I) = \Delta_{rgl}I(z, I)|_{V=0} + O(\varepsilon^2), \quad \Delta_{nls}z(z, I) = \Delta_{rglz}(z, I)|_{V=0} + O(\varepsilon^2).$$

Note that  $\Delta_{nls}I(0, I) \equiv O(\varepsilon^2)$ . We refer to [6] for more details on the Poincaré map  $\mathcal{P}$ .

We can use the map  $\mathcal{P}$  for determining the periodic orbits of (2.7). Although the periodic orbits of (2.7) correspond to traveling quasi-periodic solutions to (2.1) we do not consider these solutions for this reason. We study the periodic solutions mainly to be able to take the limit towards the homoclinic bifurcation at which the period of the solution becomes unbounded. We will use (3.2) and (3.3) to determine the curve  $\mathcal{C}_h$  in the  $(V, W)$ -plane at which those homoclinic bifurcations occur.

Note that the periodic orbits of (2.8) – the NLS case – are always  $O(\varepsilon)$  near the degenerate  $\{z = 0\}$ -plane. Thus one has to be very careful in applying the above computations, since solutions might escape to the  $\{x < 0\}$ -half space. We do not consider this problem in this paper and refer to [16] and [5] where the same problem has been considered for stationary solutions to the unperturbed Ginzburg-Landau equation (that is  $V = P = Q = 0$  in (2.8)).

We only consider the simple ‘1-circuit’ periodic orbits, which correspond to fixed points of map  $\mathcal{P}$ . Of course there might be more complex periodic orbits. Equating  $\Delta_{rgl}I$  and  $\Delta_{rglz}$  to zero yields a linear  $2 \times 2$  system in  $V$  and  $W$  with coefficients in  $T_0$  and  $T_1$ . The parameter  $P$  only appears in the inhomogeneous part of the  $2 \times 2$  system. Since both  $T_0$  and  $T_1$  diverge as  $I \rightarrow I_s$ , that is if one approaches the surface of homoclinic solutions, we divide both sides of the linear system by  $T_0 (\neq 0)$ . This way only  $\mathcal{T}$  – see (2.14) – appears in the linear system. The determinant  $\mathcal{D}$  is then given by

$$(3.5) \quad \mathcal{D}(I, z) = \frac{1}{3}\mathcal{T}^2 - \frac{2}{3}IT + z^2.$$

This is exactly the same determinant as has been studied in [6] for the same problem in the unperturbed Ginzburg-Landau equation (that is  $P = 0$ ). There, it has been shown that  $\mathcal{D} \neq 0$  for all  $(I, z) \in E$ , see (2.11). Although we do not intend to consider periodic solutions to (2.7) in detail in this paper, we can interpret this result in the following theorem:

**Theorem 3.1** *For every periodic solution, determined by the pair  $(I, z)$ , of the integrable system (2.9), there is a unique wave speed/frequency pair  $(V(I, z), W(I, z))$  such that this solution ‘survives’ the perturbations of (2.7); that is, for this choice of  $V$  and  $W$  there is a periodic solution to (2.7) which merges with the unperturbed  $(I, z)$  periodic solution in the limit  $\varepsilon \rightarrow 0$ .*

Notice that these periodic solutions correspond to (slowly) traveling quasi-periodic solutions to (2.1) – since  $x$  in (2.7) corresponds to  $|u|$  in (2.1). This theorem does not depend

on  $P$ , since  $P$  does not appear in  $\mathcal{D}$ . However, the boundaries of the  $(V, W)$ -region for which these periodic solutions exist is certainly influenced by  $P$ . A part of this boundary can be obtained by considering the limiting values  $(V(I, z), W(I, z))$  for  $I \rightarrow I_s$ : this way we determine the homoclinic bifurcation at which the period of the periodic solution tends to  $\infty$ . Another boundary can be obtained by determining the Hopf bifurcations at which periodic solutions are created by a local mechanism (see [6] for more details on this for the cubic ( $P = 0$ ) Ginzburg-Landau case).

The homoclinic bifurcations can be found by inverting the  $2 \times 2$  matrix, using approximation (2.15) of  $\mathcal{T}(I_s - \delta, z)$ , and taking the limit  $\delta \rightarrow 0$ . These computations yield for every  $P$  a curve in the  $(V, W)$ -plane, this is the curve  $\mathcal{C}_h$  of homoclinic bifurcations:

$$(3.6) \quad \mathcal{C}_h = \{(V, W) = (V_h(X), W_h(X)), X = X_s \in (\frac{2}{3}, 1)\} \text{ where}$$

$$V_h(X) = \pm \frac{2}{5}(5 + 8P - 2PX)\sqrt{1 - X},$$

$$W_h(X) = -2 + X - \frac{1}{5}P(16 - 20X + 9X^2).$$

Crossing this curve at a point  $(V_h(X), W_h(X))$  corresponds to creating or annihilating a periodic solution in (2.7) at (or better:  $O(\varepsilon)$  near) the unperturbed homoclinic solution in the  $\{z = \pm X\sqrt{1 - X}\}$ -plane (see (2.11)). Of course (3.6) is only the leading order approximation of  $\mathcal{C}_h$ .

### 3.2 The stable and unstable manifolds of ,

Map  $\mathcal{P}$  can be used for the analysis of solutions which are not (too) near to the stable and the unstable manifolds of the slow manifold , ,  $W^s(, )$  and  $W^u(, )$ . The main goal of this paper is to find heteroclinic connections  $\gamma_{\text{het}}(t)$  between (perturbed) saddle points  $S_1$  and  $S_2$  (these solutions correspond to traveling localised solutions to (1.1) which approach a stable pattern at  $x \rightarrow \pm\infty$ , subsection 2.1). Since  $S_{1,2} \in ,$  it is clear that  $\gamma_{\text{het}}(t) \in W^s(, ) \cap W^u(, )$ . Thus, understanding the behaviour of  $W^s(, )$  and  $W^u(, )$  is crucial in finding the solutions  $\gamma_{\text{het}}(t)$ . These manifolds can be studied by the Melnikov method for systems with slowly varying parameters as is presented in [28] (cf. [32]). However, first some attention should be paid to the definition of  $W^s(, )$  and  $W^u(, )$ .

The straightforward definition of  $W^s(, )$  (resp.  $W^u(, )$ ) is:  $W^s(, )$  ( $W^u(, )$ ) is the collection of all orbits (of (2.7) or (2.8)) which approach , for  $t \rightarrow \infty$  (resp.  $t \rightarrow -\infty$ ). The problem with this definition is that it is not clear how and whether , extends beyond the curve of saddle points of the integrable system. This can be illustrated by the exact solution found in [15] for the Ginzburg-Landau equation: it is a (stationary) homoclinic orbit to the degenerate critical point  $(0, 0, 0)$  of (2.7) – with  $P = V = 0$  – which is  $O(\varepsilon)$  near the curve of saddle points and to the curve of center points of the integrable limit, so the flow on this curve is everywhere  $O(\varepsilon)$  slow (see [5] for the details, see Remark 3.1). Thus, this curve coincides with , for this parameter combination. However, only near the saddles there are strong (that is  $O(1)$ ) stable and unstable directions to , . To avoid these complications we only consider the part of , which is  $O(\varepsilon)$  near the curve of unperturbed

saddles and more than a distance  $\delta$  – for some  $0 \ll \varepsilon \ll \delta \ll 1$  – away from the degenerations at  $z = \pm\sqrt{\frac{4}{27}}$ . Consider orbits  $\gamma_d(t)$  with  $\gamma_d(0)$  a distance  $> O(\varepsilon)$  away from  $\sigma$ . The stable manifold of  $\sigma$  is now defined as the collection of orbits  $\gamma_d(t)$  which are exponentially – that is  $O(e^{-\frac{\delta\lambda}{\varepsilon}})$  for some  $O(1)$  constant  $\lambda > 0$  – close to  $\sigma$ , for  $0 < \frac{\delta}{\varepsilon} < t < t_1$ , where  $t_1$  is either  $\infty$  or such that the  $z$ -coordinate of  $\gamma_d(t)$  equals  $\sqrt{\frac{4}{27}} - \delta$  or  $-\sqrt{\frac{4}{27}} + \delta$  at  $t = t_1$ . This way,  $\gamma_d(t)$  has ‘traveled’ at least a distance of  $O(\delta)$  exponentially close to  $\sigma$ , before it reached an ‘endpoint’ of  $\sigma$  (if it reaches such an endpoint). Note that by this definition  $W^s(\sigma)$  is not necessarily a two-dimensional surface, but can have an exponentially small –  $O(e^{-\frac{\delta\lambda}{\varepsilon}})$  – thickness. Finally, we only consider that part of  $W^s(\sigma)$  which merges with the surface of homoclinic solutions of the unperturbed system (Figure 1). The definition of  $W^u(\sigma)$  is analogous.

This modification has no influence on the validity (or the proof) of the Melnikov method. Moreover, the main application of this method will be for parts of  $\sigma$ , which are bounded by critical points: then  $t_1 = \infty$  and  $W^s(\sigma)$  and  $W^u(\sigma)$  are (unmodified) two-dimensional surfaces between the strong stable and unstable manifolds of these perturbed saddles. Note that –  $O(\varepsilon)$  near the  $\{z = 0\}$ -plane – there will be one degenerate ‘separatrix’ solution on  $W^s(\sigma)$  and one on  $W^u(\sigma)$ , which crosses through the  $\{x = 0\}$  plane (see [5]).

The Melnikov method for slowly varying systems measures the distance, as function of  $z$ , between the first intersections  $\mathcal{P}(\sigma)$  and  $\mathcal{P}^{-1}(\sigma)$  of  $W^u(\sigma)$  (resp.  $W^s(\sigma)$ ) with the (half-)plane  $\{y = 0, x < x_c\}$  – where  $x_c = x_c(z)$  is the  $x$ -coordinate of the unperturbed center point (see Figure 2, section 4; note that the  $\mathcal{P}$  in  $\mathcal{P}(\sigma)$  and  $\mathcal{P}^{-1}(\sigma)$  corresponds with only half of the  $\mathcal{P}$  defined in section 3.1). We define  $x_\varepsilon^u$  and  $x_\varepsilon^s$  as the intersections of  $\mathcal{P}(\sigma)$  (resp.  $\mathcal{P}^{-1}(\sigma)$ ) with  $\{z = z_0\}$ , where we assume that  $z_0 \neq 0$  – due to the modified definitions of  $W^u(\sigma)$  and  $W^s(\sigma)$  these points are not uniquely determined, but up to an exponentially small ‘error’. Solutions  $\gamma_\varepsilon^u(t) = (x_\varepsilon^u(t), y_\varepsilon^u(t), z_\varepsilon^u(t))$  in  $W^u(\sigma)$  and  $\gamma_\varepsilon^s(t) = (x_\varepsilon^s(t), y_\varepsilon^s(t), z_\varepsilon^s(t))$  in  $W^s(\sigma)$  of (2.7) or (2.8) are determined by the initial condition  $\gamma_\varepsilon^{u,s}(0) = (x_\varepsilon^{u,s}, 0, z_0)$ ;  $\gamma_0(t) = (x_h(t), y_h(t), z_0)$ : see (2.16), the homoclinic solution to the unperturbed system (2.9) with  $\gamma_0(0) = (x_m(z_0), 0, z_0)$ , where  $0 < x_m = \sqrt{2(1 - X_s)}$  is the intersection of  $\gamma_0$  with the  $x$ -axis (which does not exist for  $z_0 = 0$ , see (2.16), Figure 1). We define the following time-dependent weighted distance function ([28])

$$\Delta_\varepsilon(t, z_0) = \left( \begin{array}{c} \frac{\partial}{\partial \varepsilon}[x_\varepsilon^u(t) - x_\varepsilon^s(t)]|_{\varepsilon=0} \\ \frac{\partial}{\partial \varepsilon}[y_\varepsilon^u(t) - y_\varepsilon^s(t)]|_{\varepsilon=0} \end{array} \right) \wedge \left( \begin{array}{c} y_h(t) \\ -x_h(t) + x_h^3(t) + \frac{z_0^2}{x_h^3(t)} \end{array} \right),$$

where the wedge denotes the standard planar cross product. Thus,  $\Delta_\varepsilon(0, z_0)$  measures the  $O(\varepsilon)$  part of the distance between  $\mathcal{P}(\sigma)$  and  $\mathcal{P}^{-1}(\sigma)$  on the  $\{z = z_0\}$  axis. Note that  $\Delta_\varepsilon(0, z_0) > 0$  yields that  $x_\varepsilon^u - x_\varepsilon^s > 0$ . Using the expression for the Melnikov function derived in [28] we find that, near the RGL limit

$$(3.7) \quad \Delta_{, rgl}(0, z) = - \int_{-\infty}^{\infty} y_h [V y_h + Q x_h^5 + \frac{2z}{x_h^3} \frac{\partial z}{\partial \varepsilon}] dt,$$

where

$$(3.8) \quad \frac{d}{dt} \left( \frac{\partial z}{\partial \varepsilon} \right) = W x_h^2 + x_h^4 + P x_h^6 + V z \quad \text{and} \quad \frac{\partial z}{\partial \varepsilon} = 0 \quad \text{at} \quad t = 0.$$

By (2.16) it is possible to determine an explicit expression for  $\Delta,_{rgl}$ , which we again parametrise by  $X = X_s(z)$ :

$$(3.9) \quad -\frac{15}{4}\sqrt{2}\Delta,_{rgl}(0, z) = 5V \pm [27PX^2 - (15 + 56P)X + (15W + 20 + 32P)]\sqrt{1 - X},$$

where the  $\pm$  is again caused by  $z = \pm X\sqrt{1 - X}$ , see (2.11). The derivation of (3.9) is not completely straightforward and is therefore sketched in an appendix. Analogous to (3.4) we have

$$(3.10) \quad \Delta,_{nls}(z) = \Delta,_{rgl}(z)|_{V=0},$$

Note that all expressions are independent of  $Q$ : we can conclude that  $Q$  does not have any leading order effect on the flow generated by (2.7) or (2.8). The same is true for  $V$  in the NLS limit. Therefore, (2.8) can be considered as a subcase of (2.7) since the systems coincide at  $V = 0$ .

Based on a completely different point of view it is now possible to once again determine  $\mathcal{C}_h$ . The periodic orbit ‘needs’ at least one critical point on  $\Sigma$ , in order to ‘disappear’ as its period tends to  $\infty$  (the orbit itself remains bounded, thus the speed along the orbit must go to zero at at least one point). As a consequence, the orbit also merges with both  $W^s(\cdot)$  and  $W^u(\cdot)$  as one crosses  $\mathcal{C}_h$  in the parameter plane. Therefore,  $\mathcal{C}_h$  can be derived by combining  $\Delta,_{rgl}(0, z) = 0$  with (2.17). Instead of doing so, we can also use (3.6) to check (3.9) – or vice versa:  $\Delta,_{rgl}(0, z)$  must be equal to 0 for all  $X \in (\frac{2}{3}, 1)$  if we substitute  $V_h(X)$  and  $W_h(X)$  (3.6) into (3.9).

Expression (3.9) measures the relative position of  $W^s(\cdot)$  and  $W^u(\cdot)$ . One expects drastic changes in the global flow induced by (2.7) if the number of zeros of  $\Delta, = 0$  changes. Two such zeros are created/annihilated when an extremum of the curve (3.9) becomes tangent to the  $X$ -axis:  $W^s(\cdot)$  and  $W^u(\cdot)$  intersect non-transversely at this bifurcation. We define the curve  $\mathcal{C}_t(P)$  in the  $(V, W)$ -plane on which this bifurcation occurs:

$$(3.11) \quad \mathcal{C}_t = \{(V, W) = (V_t(X), W_t(X)), X = X_s \in (\frac{2}{3}, 1)\} \text{ where}$$

$$V_t(X) = \pm \frac{2}{5}(-15 - 56P + 54PX)(1 - X)\sqrt{1 - X},$$

$$W_t(X) = \frac{1}{15}(-50 - 144P + 45X + 276PX - 135PX^2).$$

Another way to annihilate zeros of  $\Delta,$  is by letting a zero approach the boundary  $X = \frac{2}{3}$  (that is  $z = \pm\sqrt{\frac{4}{27}}$ ) of  $\Sigma$ . This way, one finds a bifurcation curve which coincides exactly with  $\mathcal{C}_d$  (2.19), the curve at which critical points approach the same boundary! Thus, it seems that the bifurcation of critical points at  $X = \frac{2}{3}$  is coupled to the bifurcation of zeros of  $\Delta,_{rgl}(0, z)$  at the same point. One should perform a detailed analysis of the flow of (2.7) near this degenerate point in order to understand this phenomenon. We will not do so in this paper.

**Remark 3.1** The slow manifold solution constructed in [15], which is close to the curve of all – saddle and centre – critical points of the unperturbed system – see Figure 1 –

has been studied in [20] in the context of the cubic Ginzburg-Landau equation. There it is shown that the dynamics near this 1-pulse solution, for instance, can be described by a shift map. Thus, many  $N$ -pulse solutions exist. Although this analysis is completely independent of the analysis in this paper, it strongly indicates that , , or solutions which are exponentially close to it, will be connected to the degenerate critical point  $(0,0,0)$  of (2.7) for certain parameter combinations, thus yielding ‘pulse’ or ‘front’ solutions of increasing complexity.

## 4 A geometrical approach

### 4.1 Homoclinic bifurcations and the hidden symmetry

In this (sub)section we develop a geometrical interpretation of the hidden symmetry in the (cubic) Ginzburg-Landau equation – as described in the Introduction – and study its relation to the homoclinic bifurcations described in section 3. There is a strong connection between the hidden symmetry – or better: the Bekki & Nozaki solutions (1.2) – and the intersections of the two bifurcation surfaces  $\mathcal{C}_{sn}(P)$  and  $\mathcal{C}_h(P)$  in the  $(V, W, P)$  parameter space. Generically, these surfaces will intersect at a (number of) co-dimension 2 bifurcation curve(s). Equivalently, if  $P$  is kept fixed, one expects a (finite number of) intersection point(s) of  $\mathcal{C}_{sn}(P)$  and  $\mathcal{C}_h(P)$ . Now, we observe that for  $P = 0$   $\mathcal{C}_{sn}(P) = \mathcal{C}_h(P)$ ! Thus, the case  $P = 0$  – that is, the cubic Ginzburg-Landau equation – is degenerate in the sense that the homoclinic bifurcations seems to be ‘coupled’ to the saddle-node bifurcations. However, one has to be aware of the fact that both  $\mathcal{C}_{sn}$  and  $\mathcal{C}_h$  are only known up to  $O(\varepsilon)$ . Thus, the co-dimension 2 curve in  $(V, W, P)$ -space is not necessarily at  $P \equiv 0$ . Moreover,  $\mathcal{C}_{sn}$  and  $\mathcal{C}_h$  do not intersect but are tangent at  $P = 0$  (see also section 5). In this subsection we investigate the implications of this co-dimension 2 ‘coupling’ of the homoclinic and saddle-node bifurcations and determine its relation with the hidden symmetry and/or the Bekki & Nozaki solutions. Our main conclusions will be:

*All homoclinic bifurcations are of co-dimension 2 in the (cubic) Ginzburg-Landau case. The Bekki & Nozaki solutions are the heteroclinic solutions which exist at such a bifurcation.*

In order to understand the relation between the intersections of  $\mathcal{C}_{sn}$  and  $\mathcal{C}_h$  and the Bekki & Nozaki solutions (1.2) we need a geometrical framework by which we can study the flow governed by (2.7) at, and near, the homoclinic bifurcation. Before doing so, we observe that  $\mathcal{C}_h$  and  $\mathcal{C}_{sn}$  cannot intersect transversely at the co-dimension 2 bifurcation. As in subsection 3.2 we note that there must be at least one critical point ‘near’ the periodic orbit as one approaches the homoclinic bifurcation through parameter space. Hence, there cannot be a homoclinic bifurcation when this critical point has disappeared by a saddle-node bifurcation:  $\mathcal{C}_{sn}$  and  $\mathcal{C}_h$  cannot intersect transversely, unless the system has more than two critical points and the homoclinic bifurcation occurs at a critical point which is not involved in the saddle-node bifurcation. Such a transverse intersection is not a true co-dimension 2 phenomenon (this actually happens for certain  $P$ , see section 5).

Consider two (perturbed) saddle points  $S_1 = (x_1, y_1, z_1)$  and  $S_2 = (x_2, y_2, z_2)$  on , . A het-



eroclinic connection between these points is an orbit  $\gamma(t)$  in the intersection of the unstable (resp. stable) manifold of  $S_1$ ,  $W^u(S_1)$  ( $W^s(S_1)$ ), and the stable (unstable) manifold of  $S_2$ ,  $W^s(S_2)$  ( $W^u(S_2)$ ). Note that, since  $S_{1,2} \in \Sigma$ ,  $W^u(S_{1,2}) \subset W^u(\Sigma)$  and  $W^s(S_{1,2}) \subset W^s(\Sigma)$ , thus  $\gamma(t) \in W^u(\Sigma) \cap W^s(\Sigma)$  (see Figure 2). The geometrical structure of these intersections can be studied by the intersections of  $\gamma(t)$ ,  $W^u(\Sigma)$  and  $W^s(\Sigma)$  with the  $\{y = 0, x < x_c\}$ -plane. As in subsection 3.2 we define  $\mathcal{P}(\Sigma)$  (resp.  $\mathcal{P}^{-1}(\Sigma)$ ) as the first intersection of  $W^u(\Sigma)$  ( $W^s(\Sigma)$ ) with  $\{y = 0, x < x_c\}$  (Figure 2). We now assume that  $\mathcal{P}(\Sigma) \cap \mathcal{P}^{-1}(\Sigma) \neq \emptyset$  – that is we assume that  $\Delta_{\text{reg}}(0, z) = 0$  for a certain  $z = z_{\text{int}}(0)$  with  $z_2 < z_{\text{int}}(0) < z_1$  – and define  $\gamma_{\text{int}}(t) \in W^u(\Sigma) \cap W^s(\Sigma)$  such that  $\gamma_{\text{int}}(0) = (x_{\text{int}}(0), 0, z_{\text{int}}(0)) = \mathcal{P}(\Sigma) \cap \mathcal{P}^{-1}(\Sigma)$ . Orbit  $\gamma_{\text{int}}(t)$  is structurally stable, since it is an intersection of two two-dimensional manifolds. Furthermore, since  $z_2 < z_{\text{int}}(0) < z_1$ ,  $\gamma_{\text{int}}(t)$  is a so-called 1-circuit heteroclinic connection between  $S_1$  and  $S_2$ : it consists of a part  $O(\varepsilon)$  near the unperturbed homoclinic orbit in the  $\{z = z_{\text{int}}(0)\}$ -plane and two parts ‘above’ and ‘below’  $\{z = z_{\text{int}}(0)\}$ , exponentially close to  $\Sigma$ . (Figure 2). It depends on the direction of the flow on  $\Sigma$ , between  $S_1$  and  $S_2$  whether  $\gamma_{\text{int}}(t)$  goes, for increasing  $t$ , from  $S_1$  to  $S_2$  or vice versa. In Figure 2 we choose  $\dot{z} < 0$  on  $\Sigma$ , between  $S_1$  and  $S_2$ , thus  $\gamma_{\text{int}}(t) = W^u(S_1) \cap W^s(S_2)$  and  $\lim_{t \rightarrow -\infty} \gamma_{\text{int}}(t) = S_1$ ,  $\lim_{t \rightarrow \infty} \gamma_{\text{int}}(t) = S_2$ . Note that  $W^u(S_1) \neq W^u(\Sigma)$  and  $W^s(S_2) \neq W^s(\Sigma)$ :  $W^u(S_1)$  is bounded from below by  $W^u(S_2)$  – a one-dimensional manifold – and  $W^s(S_2)$  has  $W^s(S_1)$  as (one-dimensional) upper-boundary (Figure 2). These boundaries are no subsets of the two-dimensional manifolds. The relative positions of  $z_2$ ,  $z_{\text{int}}(0)$  and  $z_1$  changes if one varies the parameters in the problem. By subsection 3.2 we know that the homoclinic bifurcation appears as one of the saddles  $S_{1,2}$  approaches the  $\{z = z_{\text{int}}(0)\}$ -plane.

We can now see how the homoclinic solution is created from the heteroclinic solution at the homoclinic bifurcation: as  $S_{1,2}$  approaches the  $\{z = z_{\text{int}}(0)\}$ -plane  $\gamma_{\text{int}}(t)$  approaches a boundary of the two-dimensional stable/unstable manifolds of  $S_{1,2}$ . In the case represented by Figure 2 there is a homoclinic bifurcation either as  $\gamma_{\text{int}}(t) = W^u(S_2)$  or  $\gamma_{\text{int}}(t) = W^s(S_1)$ . In the former case  $\gamma_{\text{int}}(t)$  has become a homoclinic solution to  $S_2$  and is the intersection of a two-dimensional manifold  $W^s(S_2)$  and a one-dimensional manifold  $W^u(S_2)$ , in the latter case  $\gamma_{\text{int}}(t) \in W^u(S_1) \cap W^s(S_1)$ , also a non-structurally stable homoclinic orbit. Both homoclinic orbits can be seen as the product of a co-dimension 1 bifurcation. Note that this really is the homoclinic bifurcation as described in subsection 3.1: at the bifurcation,  $\gamma_{\text{int}}(t)$  is the limit of the ‘disappearing’ periodic solution.

These structurally stable heteroclinic solutions  $\gamma_{\text{int}}(t)$  of the above type also exist for  $(V, W)$  in a certain (open) region of the parameter plane in the cubic Ginzburg-Landau case ( $P = 0$ ). This can be concluded by combining (2.17) and (3.6) for  $P = 0$  which will be done in detail in subsection 5.2. It can be checked that – unlike in Figure 2 – the flow on  $\Sigma$ , goes from  $S_2$  to  $S_1$ , in this case. Thus,  $\gamma_{\text{int}}(t)$  is a (structurally stable) heteroclinic connection between  $S_2$  and  $S_1$ :  $\gamma_{\text{int}}(t) \in W^s(S_1) \cap W^u(S_2)$ . One expects homoclinic orbits at (some of) the boundaries of this region of structurally stable heteroclinic solutions. There are two co-dimension 1 homoclinic bifurcations possible in this situation: either  $\gamma_{\text{int}}(t)$  becomes a homoclinic solution to  $S_1$  as  $|z_1 - z_{\text{int}}(0)|$  becomes  $O(\varepsilon)$  and  $\gamma_{\text{int}}(t)$  merges with the one-dimensional manifold  $W^u(S_1)$ , a boundary of  $W^u(S_2)$ , or,  $\gamma_{\text{int}}(t)$  becomes a homoclinic solution to  $S_2$  as  $|z_{\text{int}}(0) - z_2|$  becomes  $O(\varepsilon)$  and  $\gamma_{\text{int}}(t) = W^s(S_2)$ , a boundary of  $W^s(S_1)$  (Figure 3).

In both co-dimension 1 cases we have to assume that the other saddle is  $O(1)$  away from the plane in which the bifurcation occurs. This assumption is crucial: ‘in between’ both co-dimension 1 situations is the co-dimension 2 ‘homoclinic/saddle-node’ bifurcation at which both  $S_1$  and  $S_2$  are  $O(\varepsilon)$  near the  $\{z = z_{\text{int}}(0)\}$ -plane. At this bifurcation  $\gamma_{\text{int}}(t)$  is both on a boundary of  $W^u(S_2)$  and on a boundary of  $W^s(S_1)$ :  $\gamma_{\text{int}}(t) = W^u(S_1) = W^s(S_2)$ , a connection between two one-dimensional manifolds (Figure 3);  $\gamma_{\text{int}}(t)$  still is a heteroclinic connection between  $S_1$  and  $S_2$ , but that it now goes the other way, from  $S_1$  to  $S_2$ . This is the co-dimension 2 bifurcation that occurs as  $\mathcal{C}_h$  and  $\mathcal{C}_{sn}$  are (at least)  $O(\varepsilon)$  close (since  $|z_1 - z_2| = O(\varepsilon)$ , see Remark 4.1). Note that in this case the periodic orbit merges at  $\mathcal{C}_h$  with the heteroclinic cycle formed by  $\gamma_{\text{int}}(t)$  and the part of , between  $S_1$  and  $S_2$  (see [6]). Near such a co-dimension 2 point in parameter space one finds all three orbits sketched in Figure 3. The existence of this bifurcation is not influenced by the direction of the flow on , between  $S_1$  and  $S_2$ : Figure 3 has an equivalent which corresponds to the situation sketched in Figure 2.

Based on the above geometrical arguments one expects a curve of these co-dimension 2 bifurcations in the three-dimensional  $(V, W, P)$  parameter space. By the observations at the beginning of this section –  $\mathcal{C}_h = \mathcal{C}_{sn} + O(\varepsilon)$  at  $P = 0$  – we know that  $P$  must be  $O(\varepsilon)$  to find this curve. Thus, we know that there must be a curve of homoclinic co-dimension 2 bifurcations in the  $(V, W, P)$ -space  $O(\varepsilon)$  near the  $\{P = 0\}$ -plane. For parameter combinations  $(V, W, P)$  on this curve there exists in (2.7) a heteroclinic orbit which is the connection of two one-dimensional manifolds. We can now use the results of [6] to conclude that  $P$  must be  $\equiv 0$  at this curve: in [6] it has been show that the periodic solutions merge with a Bekki & Nozaki solution (1.2) at  $\mathcal{C}_h$  (in the cubic Ginzburg-Landau case). Note that it is conceptually simple to achieve this: one just has to use the explicit expressions for the Bekki & Nozaki solutions (1.2) and show that these solutions exist at  $\mathcal{C}_h$  at the correct position in the phase-space – that is ‘near’ the ‘disappearing’ periodic solution. Therefore, we do not repeat these computations here.

Thus we can once more conclude that *the homoclinic bifurcations are of co-dimension 2 in the (cubic) Ginzburg-Landau equation; the Bekki & Nozaki family of connections between two one-dimensional manifolds (see the introduction, [29], [6]) represents exactly this curve of co-dimension 2 homoclinic bifurcations.*

This geometrical approach does not give a complete explanation of the hidden symmetry as described in [29], since it does not explain why a curve of co-dimension 2 bifurcations occurs exactly for  $P = 0$ , the cubic Ginzburg-Landau case. However, the hidden symmetry can now be interpreted – and fully analysed – as a natural phenomenon occurring in bifurcation analysis. From the bifurcation theory point of view it is clear that the curve of co-dimension 2 homoclinic bifurcations must exist in  $(V, W, P)$ -space. The fact that  $P = 0$  has no influence on the investigation of this curve.

Finally, one would like to answer the question: can there be heteroclinic solutions of the Bekki & Nozaki type – that is: heteroclinic orbits which connect a one-dimensional unstable manifold of a saddle  $S$  to a one-dimensional stable manifold of a saddle  $\hat{S}$  – for

$P \neq 0$ ? This question can partly be answered by determining the full set  $\mathcal{C}_{sn} \cap \mathcal{C}_h$ . By (2.18) and (3.6) we find that this set consists of three branches: the Bekki & Nozaki branch in the  $\{P = 0\}$ -plane, a branch at  $V = 0$  with  $X \equiv 1$  and a branch with  $X \equiv \frac{2}{3}$  (see section 5.1 for explicit formulae ((5.2), (5.3)). Note that these two new branches are degenerate, in the sense that they are related to bifurcations in (or near) the degenerate planes  $\{z = 0\}$  and  $\{z = \pm\sqrt{\frac{4}{27}}\}$ . The behaviour near the latter branch must be extremely singular since the entire branch is a subset of  $\mathcal{C}_{sn} \cap \mathcal{C}_h \cap \mathcal{C}_d \cap \mathcal{C}_t$  (see section 5). Moreover, the slow manifold, is, strictly speaking, not defined near  $\{z = \pm\sqrt{\frac{4}{27}}\}$  (see subsection 3.2) and the unperturbed system is degenerate at  $X = \frac{2}{3}$  (see Figure 1). Therefore, we do not pay any attention to this branch in the paper.

In contrast to this it is possible to analyse the flow governed by the system near the real Ginzburg-Landau limit, (2.7), and the system near the nonlinear Schrödinger limit, (2.8), on the  $\{V = 0\}$ -branch of  $\mathcal{C}_{sn} \cap \mathcal{C}_h$ . First we recall that these systems are identical for  $V = 0$ , then we note that there is a simple symmetry in the systems:

$$(4.1) \quad x \rightarrow x, y \rightarrow -y, z \rightarrow -z, t \rightarrow -t.$$

This symmetry can be used to handle the degenerations near the  $\{z = 0\}$ -plane and to construct symmetric, degenerate heteroclinic orbits which connect one-dimensional stable manifolds to one-dimensional unstable manifolds. In a sense one can interpret symmetry (4.1) as the explicit version of the hidden symmetry conjectured by van Saarloos and Hohenberg [29]. Moreover, the existence of the symmetric, degenerate heteroclinic orbits does not necessarily violate the geometric counting arguments of [29] for  $V = 0$ , due to symmetry (4.1). On the contrary: the construction of these orbits is based on the symmetry. The existence of these degenerate heteroclinic orbits can be shown using the methods developed in [23] and [5]. In these papers systems are studied which are very similar to (2.7) with  $V = 0$ . In both papers the existence is shown of symmetric orbits connecting the fast unstable manifold of a saddle  $S$  with the fast unstable manifold of its symmetric counterpart  $\hat{S}$ . Moreover, it is shown that for any  $N > 0$  there is such a degenerate heteroclinic orbit which makes  $N$  excursions through the fast field (see also subsection 4.2). The methods of [23] and [5] can be applied to derive similar results for systems (2.7) and (2.8) with  $V = 0$ . However, in this paper we will not study the details of the construction of these degenerate symmetrical orbits.

We conclude this subsection by noting that we found that there cannot be non-symmetric co-dimension 2 homoclinic bifurcations of the above type for  $P \neq 0$ . In other words: *There are no heteroclinic solutions of the Bekki & Nozaki type for  $P \neq 0$ .* Thus, the introduction of a small quintic term in the cubic Ginzburg-Landau equation (as in (1.1)) truly breaks the hidden symmetry. These results will be formulated as a Theorem and a Corollary in subsection 5.2.

**Remark 4.1** In [6] it is shown that  $\mathcal{C}_{sn}$  and  $\mathcal{C}_h$  are actually  $O(\varepsilon^2)$  apart for  $P = 0$ : there is a strip of  $O(\varepsilon^2)$  width between  $\mathcal{C}_{sn}$  and  $\mathcal{C}_h$  where there are two (perturbed) saddles, but there is no heteroclinic connection between these points (yet).

## 4.2 Infinitely many structurally stable heteroclinic orbits

A traveling solution of localised structure to (2.1) or (2.2) corresponds to a heteroclinic solution  $\gamma_{\text{het}}(t)$  to (2.7) or (2.8). Such a solution  $\gamma_{\text{het}}(t)$  exists if the following conditions are satisfied:

- (i)  $W^s(\cdot) \cap W^u(\cdot) \neq \emptyset$ .
- (ii) There are at least two perturbed saddles  $S_{1,2} = (x_{1,2}, y_{1,2}, z_{1,2}) \in \Sigma$ , with  $z_2 < z_1$ .
- (iii)  $z_2 < z_{\text{int}}(0) < z_1$  and  $|z_{\text{int}}(0) - z_{1,2}| \gg \varepsilon$ , where  $z_{\text{int}}(0)$  = the  $z$ -coordinate of  $\mathcal{P}(\cdot) \cap \mathcal{P}^{-1}(\cdot)$ .

Note that we distinguish between  $\gamma_{\text{int}}(t)$ , the first intersection of  $W^s(\cdot)$  and  $W^u(\cdot)$  – which is not necessarily a heteroclinic orbit ((ii), (iii)) – and  $\gamma_{\text{het}}(t)$ . Condition (ii) can be weakened slightly since we also want to take into account homoclinic orbits to a saddle point. Note however, that such orbits can only exist at a global bifurcation (subsection 4.1), while it is clear from the above conditions that  $\gamma_{\text{het}}(t)$  is, in general, a structurally stable orbit (see subsection 4.1 and Figure 2). To avoid degenerations we assume that  $z_{\text{int}}(0)$  is not  $O(\varepsilon)$  close to either 0 or  $\pm\sqrt{\frac{4}{27}}$ .

By the results of section 3 – and in particular the expressions for the bifurcation curves  $\mathcal{C}_{sn}$ ,  $\mathcal{C}_d$ ,  $\mathcal{C}_h$  and  $\mathcal{C}_t$  – it is a rather straightforward job to determine for every  $P$  the regions in the  $(V, W)$  parameter plane where (2.7) satisfies these conditions. We will do so in section 5. In this (sub)section we consider in more detail the implications of the above conditions for the structure of  $W^s(\cdot) \cap W^u(\cdot)$ , where we pay special attention to the – so far neglected – higher order intersections.

Consider an intersection point  $(x_{\text{int}}(0), z_{\text{int}}(0)) = \mathcal{P}(\cdot) \cap \mathcal{P}^{-1}(\cdot)$  (Figure 2). Such a point corresponds to a zero of  $\Delta_{\text{rgl}}(0, z)$ . We assume that the system is not close to a homoclinic bifurcation, thus  $z_{\text{int}}(0)$  is not  $O(\varepsilon)$  close to the  $z$ -coordinate of a saddle point. One must now distinguish between two different relative positions of  $\mathcal{P}(\cdot)$  and  $\mathcal{P}^{-1}(\cdot)$  near  $(x_{\text{int}}(0), z_{\text{int}}(0))$  ( $\mathcal{P}(\cdot)$  is to the right/left of  $\mathcal{P}^{-1}(\cdot)$  for  $z$  (just) above  $z_{\text{int}}(0)$ ). Furthermore, the flow on  $\Sigma$  might go up ( $\dot{z} > 0$ ) or down ( $\dot{z} < 0$ ) at  $z = z_{\text{int}}(0)$ . Hence, there are four different situations. However, we are only concerned with the existence of the connections  $\gamma_{\text{het}}(t)$ , not with the direction of the flow on  $\gamma_{\text{het}}(t)$ . Thus, by reversing the time  $t \rightarrow -t$  we transform  $\mathcal{P}(\cdot) \rightarrow \mathcal{P}^{-1}(\cdot)$  and  $\dot{z} \rightarrow -\dot{z}$  and obtain a reduction to two – we will find – structurally different situations:

- (A)  $W^s(\cdot)$  is outside  $W^u(\cdot)$  for  $\tilde{z}$  (just) above  $z_{\text{int}}(0)$  and  $\dot{z}|_{z=\tilde{z}} > 0$   
(or  $W^s(\cdot)$  is inside  $W^u(\cdot)$  for  $\tilde{z}$  (just) above  $z_{\text{int}}(0)$  and  $\dot{z}|_{z=\tilde{z}} < 0$ ),
- (B)  $W^s(\cdot)$  is outside  $W^u(\cdot)$  for  $\tilde{z}$  (just) above  $z_{\text{int}}(0)$  and  $\dot{z}|_{z=\tilde{z}} < 0$   
(or  $W^s(\cdot)$  is inside  $W^u(\cdot)$  for  $\tilde{z}$  (just) above  $z_{\text{int}}(0)$  and  $\dot{z}|_{z=\tilde{z}} > 0$ )

(see Figure 4). Note that it is necessary to use the addition ‘just’ in the above descriptions since there might be another zero of  $\Delta_{\text{rgl}}(0, z)$  above  $z_{\text{int}}(0)$ . As we shall see in subsection 5: the cubic Ginzburg-Landau case ( $P = 0$ ) is of type (A). In the formulation and the proof of the theorem below we shall assume that  $W^s(\cdot)$  is outside  $W^u(\cdot)$  for  $\tilde{z}$  (just) above  $z_{\text{int}}(0)$  in both cases.

**Theorem 4.2** *Suppose the system (2.7) satisfies conditions (i), (ii) and (iii) for a given parameter combination  $(V, W, P)$  then*

- case (A): There is a unique (structurally stable) heteroclinic orbit  $\gamma_{\text{het}}(t) = \gamma_{\text{int}}(t) = W^s(\cdot) \cap W^u(\cdot)$  with  $\lim_{t \rightarrow -\infty} \gamma_{\text{het}}(t) = S_2$  and  $\lim_{t \rightarrow \infty} \gamma_{\text{het}}(t) = S_1$  if  $|z_{\text{int}}(0) - z_1| \gg O(\varepsilon |\log \varepsilon|)$ .*
- case (B): There are countably many structurally stable multi-circuit heteroclinic orbits  $\gamma_{\text{het}}(t) = \gamma_{\text{int}}^N(t)$ ,  $N = 1, 2, 3, \dots$  with  $\lim_{t \rightarrow -\infty} \gamma_{\text{het}}(t) = S_1$  and  $\lim_{t \rightarrow \infty} \gamma_{\text{het}}(t) = S_2$ ;  $\gamma_{\text{int}}^N(t)$  makes  $N$  excursions through the fast field,  $O(\varepsilon)$  close to a homoclinic solution of the unperturbed flow;  $\gamma_{\text{int}}(t) = \gamma_{\text{int}}^1(t)$ : the 1-circuit orbit.*

Note that the part of  $\gamma_{\text{het}}$  between  $S_1$  and  $S_2$  can be considered as a 0-circuit heteroclinic connection (in both cases).

A similar result for a model problem has been proven in [8] (cf. Theorem 4.3). The geometrical aspects of the arguments are in essence the same for both – the model problem and the perturbed Ginzburg-Landau – vector fields. However, due to a somewhat more precise perturbation analysis of the system in case (A), the above uniqueness result is a little stronger than its counterpart in [8]. Moreover, in Remark 4.5 we will show that the  $\varepsilon |\log \varepsilon|$  condition in case (A) can be deleted depending on the behaviour of the map  $\mathcal{P}$  in the fast field – subsection 3.1 – near  $(x_{\text{int}}(0), z_{\text{int}}(0))$ . In the proof, an important role will be played by the strong stable and unstable manifolds,  $W^{\text{ss}}(S_{1,2})$  and  $W^{\text{uu}}(S_{1,2})$ , of the critical points  $S_{1,2}$ . These are the one-dimensional manifolds which correspond to the  $O(1)$  eigenvalues of  $S_{1,2}$ . We define  $\mathcal{P}(S_{1,2})$  (resp.  $\mathcal{P}^{-1}(S_{1,2})$ ) as the (first) intersection of  $W^{\text{uu}}(S_{1,2})$  ( $W^{\text{ss}}(S_{1,2})$ ) with  $\{y = 0, x < x_c\}$ , see Figure 4.

**Proof:** Both in case (A) and in case (B)  $\gamma_{\text{int}}(t)$  is a structurally stable heteroclinic orbit between  $S_1$  and  $S_2$ . However, in case (A):  $\lim_{t \rightarrow -\infty} \gamma_{\text{int}}(t) = S_2$  and  $\lim_{t \rightarrow \infty} \gamma_{\text{int}}(t) = S_1$ , while  $\lim_{t \rightarrow -\infty} \gamma_{\text{int}}(t) = S_1$   $\lim_{t \rightarrow \infty} \gamma_{\text{int}}(t) = S_2$  in case (B). This difference is completely caused by the flow on  $\Sigma$ : in both cases  $\gamma_{\text{int}}(t)$  is  $O(\varepsilon)$  close to the homoclinic orbit to the unperturbed system (2.9) at  $z = z_{\text{int}}(0)$  during its circuit through the fast field.

We now consider the second intersection,  $\mathcal{P}(\mathcal{P}(\cdot)) \stackrel{\text{def}}{=} \mathcal{P}^2(\cdot)$  with return map  $\mathcal{P}$  as in subsection 3.1, of  $W^u(\cdot)$  and  $\{y = 0, x < x_c\}$ . First, we observe that the return map is only defined for points on those parts of  $\mathcal{P}(\cdot)$  which are inside  $W^s(\cdot)$ , that is, to the right of  $\mathcal{P}^{-1}(\cdot)$  (Figure 4). We consider an open segment  $\mathcal{L} \subset \mathcal{P}(\cdot)$  bounded from below by  $(x_{\text{int}}(0), z_{\text{int}}(0))$ . Thus  $\mathcal{P}(\mathcal{L})$  exists. Moreover, the image of a point  $p \in \mathcal{L}$  arbitrarily close to  $(x_{\text{int}}(0), z_{\text{int}}(0))$  can be deduced by following  $\gamma_{\text{int}}(t)$ . In case (A) the orbit  $\gamma_p$  through  $p$  follows  $\gamma_{\text{int}}(t)$  ‘upwards’ to  $S_1$  and then leaves  $\Sigma$ , along with  $W^{\text{uu}}(S_1)$ . We find

$$\lim_{p \rightarrow (x_{\text{int}}(0), z_{\text{int}}(0))} \mathcal{P}(p) = \mathcal{P}(S_1).$$

Note that, due to the slow flow along  $\Sigma$ ,  $\|p - \mathcal{P}(p)\| = O(1)$ . Analogously, we deduce that  $p$  is mapped downwards in case (B):

$$\lim_{p \rightarrow (x_{\text{int}}(0), z_{\text{int}}(0))} \mathcal{P}(p) = \mathcal{P}(S_2).$$

Now, consider a point  $p \in \mathcal{L}$  which is at a distance of  $O(\varepsilon)$  of  $(x_{\text{int}}(0), z_{\text{int}}(0))$ , and not closer than that. By assumption (iii) we know that  $p$  is below  $\mathcal{P}(S_1)$ . The orbit  $\gamma_p$  follows  $\gamma_{\text{int}}(t)$  and approaches  $\Sigma$ , up to an  $O(\sqrt{\varepsilon})$  distance. By the linearized flow near  $\Sigma$ , we find that  $\gamma_p$  remains a time interval of length  $O(|\log \varepsilon|)$  near  $\Sigma$ . Thus, as  $\gamma_p$  returns to  $\{y = 0, x < x_c\}$  it has moved an  $O(\varepsilon)$  distance by the fast field – subsection 3.1 – and an  $O(\varepsilon|\log(\varepsilon)|)$  by the slow field near  $\Sigma$ . Note that here we assumed that  $\gamma_p$  has not come close a critical point on  $\Sigma$ , (if that's the case the distance traveled along  $\Sigma$  will (can) be less than  $O(\varepsilon|\log \varepsilon|)$ ). In case (A) the latter is upwards, thus,  $\mathcal{P}(p)$  is above the  $\{z = z_{\text{int}}(0)\}$  level (here we used that  $|z_{\text{int}}(0) - z_1| \gg O(\varepsilon|\log \varepsilon|)$ ). The orbit  $\gamma_p$  remains longer near  $\Sigma$ , if  $p$  gets closer to  $(x_{\text{int}}(0), z_{\text{int}}(0))$ , which yields that  $\mathcal{P}(p)$  will be further away from  $\{z = z_{\text{int}}(0)\}$ . If the distance of  $p$  to  $(x_{\text{int}}(0), z_{\text{int}}(0))$  is larger than  $O(\varepsilon)$  the influence of the fast field on  $\mathcal{P}(p)$  increases but, since this effect is always  $O(\varepsilon)$ ,  $\mathcal{P}(p)$  will be more than  $O(\varepsilon)$  away from  $\{z = z_{\text{int}}(0)\}$ . We conclude that  $\mathcal{P}(\mathcal{L}) \cap \{z = z_{\text{int}}(0)\} = \emptyset$  in case (A). As a consequence we observe that  $\mathcal{P}^2(\Sigma) \cap \mathcal{P}^{-1}(\Sigma) = \emptyset$  (see Figure 4a). Exactly the same arguments can be applied for the flow with reversed time and we conclude:  $\mathcal{P}^{-1}(\mathcal{P}^{-1}(\Sigma)) \stackrel{\text{def}}{=} \mathcal{P}^{-2}(\Sigma)$  remains below  $\{z = z_{\text{int}}(0)\}$  and thus  $\mathcal{P}^{-2}(\Sigma) \cap \mathcal{P}(\Sigma) = \emptyset$  and  $\mathcal{P}^{-2}(\Sigma) \cap \mathcal{P}^2(\Sigma) = \emptyset$  in case (A) (Figure 4a).

Due to the downward direction on  $\Sigma$ ,  $\mathcal{P}^2(\Sigma)$  (and  $\mathcal{P}^{-2}(\Sigma)$ ) must behave completely different in case (B). The images of points  $p \in \mathcal{L}$  close enough to  $(x_{\text{int}}(0), z_{\text{int}}(0))$  will be outside – that is to the left of  $-\mathcal{P}^{-1}(\Sigma)$ . In contrast with this, we deduce, by the above arguments, that  $\mathcal{P}(p)$  is inside (right) of  $\mathcal{P}^{-1}(\Sigma)$  if the distance between  $p$  and  $(x_{\text{int}}(0), z_{\text{int}}(0))$  is large enough. Thus  $\mathcal{P}^2(\Sigma) \cap \mathcal{P}^{-1}(\Sigma) \neq \emptyset$  and – by reversing time:  $\mathcal{P}^{-2}(\Sigma) \cap \mathcal{P}(\Sigma) \neq \emptyset$ ,  $\mathcal{P}^{-2}(\Sigma) \cap \mathcal{P}^2(\Sigma) \neq \emptyset$  (Figure 4b). Thus there exists an orbit  $\gamma_{\text{int}}^2(t)$  with  $\lim_{t \rightarrow -\infty} \gamma_{\text{int}}^2(t) = S_1$  which is exponentially close to  $\Sigma$ , except for two circuits through the fast field: during the first circuit it passes through  $\mathcal{P}(\Sigma) \cap \mathcal{P}^{-2}(\Sigma)$  on  $\{y = 0, x < x_c\}$ , after which it is again close to  $\Sigma$ , until the second circuit during which it passes through  $\mathcal{P}^2(\Sigma) \cap \mathcal{P}^{-1}(\Sigma)$ ; then it returns to  $\Sigma$ , and approaches  $S_2$  as  $t \rightarrow \infty$ . This is the first structurally stable –  $\gamma_{\text{int}}^2(t)$  is an intersection of two two-dimensional manifolds – ‘multi’-circuit heteroclinic solution as presented in the theorem.

Next, we consider the third, etc. intersections of  $W^u(\Sigma)$  and  $W^s(\Sigma)$  (for reversed time) with  $\{y = 0, x < x_c\}$ . We note that in both cases the distance between a point on  $\mathcal{P}^2(\Sigma)$  (resp.  $\mathcal{P}^{-2}(\Sigma)$ ) and  $\mathcal{P}(\Sigma)$  ( $\mathcal{P}^{-1}(\Sigma)$ ) cannot exceed  $O(\varepsilon)$ .

First, we study case (A). We observe that the minimum  $M_2$  of the  $\mathcal{P}^2(\Sigma)$ -‘tongue’ is  $O(\varepsilon|\log \varepsilon|)$  above  $\{z = z_{\text{int}}(0)\}$ . Thus, the orbit through  $M_2$ ,  $\gamma_M$ , will come  $O(\sqrt{\varepsilon})$  close to  $\Sigma$ ,  $O(\varepsilon|\log \varepsilon|)$  above  $\{z = z_{\text{int}}(0)\}$ . The slow flow on  $\Sigma$ , will again ‘lift’  $\gamma_M$   $O(\varepsilon|\log \varepsilon|)$ . The same is true for for points  $O(\varepsilon)$  close to  $M_2$ , thus,  $\mathcal{P}^3(\Sigma)$  will also be a tongue, ‘stitched’ to  $\mathcal{P}^2(S_1)$  (the second intersection of  $W^{\text{uu}}(S_1)$  with  $\{y = 0, x < x_c\}$ ) with a minimum  $M_3$   $O(\varepsilon|\log \varepsilon|)$  above  $M_2$  (Figure 4a). The same arguments can be applied to  $\mathcal{P}^4(\Sigma)$ ,  $\mathcal{P}^{-3}(\Sigma)$  etc., thus we conclude that  $W^u(\Sigma)$  and  $W^s(\Sigma)$  have a unique intersection: the heteroclinic orbit  $\gamma_{\text{het}}(t) = \gamma_{\text{int}}(t)$ .

In case (B), we first note that only orbits through the part of  $\mathcal{P}^2(\Sigma)$  to the right of  $\mathcal{P}^{-1}(\Sigma)$  will have a next intersection with  $\{y = 0, x < x_c\}$ . This part of  $\mathcal{P}^2(\Sigma)$  is bounded

from below by  $\gamma_{\text{int}}^2(0)$ , the second intersection of  $\gamma_{\text{int}}^2(t)$  with  $\{y = 0, x < x_c\}$ . By letting  $\gamma_{\text{int}}^2(t)$  play the role of  $\gamma_{\text{int}}(t)$  (for  $t > 0$ ) we see that we can repeat the arguments by which we derived the structure of  $\mathcal{P}^2(\cdot, \cdot)$ :  $\mathcal{P}^3(\cdot, \cdot)$  is also stitched to  $\mathcal{P}(S_2)$  and intersects  $\mathcal{P}^{-1}(\cdot, \cdot)$  in a point below  $\gamma_{\text{int}}^2(t)$ . This point,  $\gamma_{\text{int}}^3(0)$ , is the last intersection point of the (structurally stable) 3-circuit heteroclinic orbit  $\gamma_{\text{int}}^3(t)$  with  $\{y = 0, x < x_c\}$ . The other two intersection points are  $\mathcal{P}(\cdot, \cdot) \cap \mathcal{P}^{-3}(\cdot, \cdot)$  – the structure of  $\mathcal{P}^{-3}(\cdot, \cdot)$  can be obtained along the above lines (Figure 4b) – and  $\mathcal{P}^2(\cdot, \cdot) \cap \mathcal{P}^{-2}(\cdot, \cdot)$ . The higher order intersections  $\mathcal{P}^N(\cdot, \cdot)$ ,  $N = 4, 5, \dots$  all intersect  $\mathcal{P}^{-1}(\cdot, \cdot)$ , which yields that there must be a (countably) infinite collection of (structurally stable)  $N$ -circuit heteroclinic orbits  $\gamma_{\text{int}}^N(t) \in W^u(\cdot, \cdot) \cap W^s(\cdot, \cdot)$  which all connect  $S_1$  to  $S_2$ .  $\square$

In the next section we will investigate for which values of  $P$  there exist parameter combinations  $(V, W)$  such that the system satisfies (i), (ii) and (iii) so that we can apply Theorem 4.2. In this paper we do not pay much attention to the fate of the higher order intersections of  $W^s(\cdot, \cdot)$  and  $W^u(\cdot, \cdot)$  as  $z_{\text{int}}(0)$  approaches  $S_1$  or  $S_2$ . These bifurcations has been studied in [8] – for a model problem – and it has been show there that infinitely many orbits  $\gamma_{\text{int}}^N$  of case (B) are created at once, that is, at the bifurcation there is a *homoclinic explosion*. Analogously, the unique intersection  $\gamma_{\text{int}}(t)$  can be seen as the result of a *homoclinic implosion*. These results will also hold for the flow induced by (2.7), since the arguments are in essence of a geometrical nature.

Note that if there is a third saddle  $\hat{S}_1$  on  $\Sigma$ , above  $S_1$  and if  $\mathcal{C}_h$  has been crossed so that  $z_{\text{int}}(0)$  has passed  $z_1$ , one can apply Theorem 4.2 to the intersection(s) of  $W^s(\cdot, \cdot)$  and  $W^u(\cdot, \cdot)$  between  $\hat{S}_1$  and  $S_1$ . Since the direction of the flow on  $\Sigma$  must be opposite to the direction of the flow between  $S_1$  and  $S_2$  we find that a case (A) situation has been changed into a case (B) situation by crossing  $\mathcal{C}_h$  and vice versa. This explains why we can interpret the unique intersection  $\gamma_{\text{int}}(t)$  in case (A) as the result of an implosion. Since we will encounter this phenomenon frequently in section 5 we formulate it as a corollary:

**Corollary 4.3** *Let there be three critical points  $S_1 = (x_1, y_1, z_1)$ ,  $S_2 = (x_2, y_2, z_2)$  and  $S_3 = (x_3, y_3, z_3)$  on  $\Sigma$ , with  $z_1 > z_2 > z_3$  and not  $O(\varepsilon|\log \varepsilon|)$  close, and let  $\Delta$ ,  $r_{\text{gl}}(0, z)$  have a zero  $z_\Delta$  between  $z_3$  and  $z_1$ . If  $z_2$  and  $z_\Delta$  pass each other as  $\mathcal{C}_h$  is crossed in the  $(V, W)$  plane, then the type of the heteroclinic orbit(s)  $\gamma_{\text{het}}(t)$  described in Theorem 4.2 has changed from case (A) to (B) or vice versa.*

**Remark 4.4** Note that an intersection of  $W^u(\cdot, \cdot)$  and  $W^s(\cdot, \cdot)$  of type (B) also induces higher order intersections if  $z_{\text{int}}(0)$  is not bounded from above and below by  $z_{1,2}$  (cf. (ii)). These intersections can be regarded as (multiple-circuit) homoclinic solutions to  $\Sigma$ . The behaviour of these solutions in the limits  $t \rightarrow \pm\infty$  is completely coupled to the behaviour of  $\Sigma$ , outside the  $z$ -interval  $[-\sqrt{\frac{4}{27}} + \delta, \sqrt{\frac{4}{27}} - \delta]$  (see Remark 3.1).

**Remark 4.5** In [8] a distinction has been made between four instead of two cases: if one studies case (A) and case (B) near the explosive/implosive bifurcation one finds that the accumulated influence of the fast field during one circuit causes an important difference. This can be seen by reconsidering the condition  $|z_{\text{int}}(0) - z_1| \gg O(\varepsilon|\log \varepsilon|)$  in case (A) of the theorem. This condition is necessary because if  $z_{\text{int}}(0)$  gets nearer to  $z_1$  the

slow field induces less than an  $O(\varepsilon|\log \varepsilon|)$  lift for orbits which start  $O(\varepsilon)$  near  $\gamma_{\text{int}}(t)$  in  $\{y = 0, x < x_c\}$ , so the influence of the fast field might create an intersection of  $\mathcal{P}^2(\cdot, \cdot)$  with  $\{z = z_{\text{int}}(0)\}$  and thus:  $\mathcal{P}^2(\cdot, \cdot) \cap \mathcal{P}^{-2}(\cdot, \cdot) \neq \emptyset$ . This will not happen if the fast field also has an upwards effect. Since  $O(\varepsilon)$  changes in the initial condition do not have a leading order effect on the fast field part of return map  $\mathcal{P}$  – subsection 3.1 – we know that the fast field has an upwards effect near the bifurcation if the  $z$ -coordinate of  $\mathcal{P}(S_1)$  is larger than  $z_1$ , the  $z$ -coordinate of  $S_1$ . If this is the case it can be shown quite easily – the proof will be very similar to that for the model problem in [8] – that the homoclinic implosion occurs exactly at  $\mathcal{C}_h$ , the curve at which the periodic solution merges with a homoclinic solution. If this is not the case, the bifurcation is more complicated: there will be (infinitely many) intersections of  $W^u(\cdot, \cdot)$  and  $W^s(\cdot, \cdot)$  – related to heteroclinic orbits which make many excursions through the fast field – and secondary implosions (or explosions) before one crosses  $\mathcal{C}_h$ . These bifurcations have not been studied in detail yet, and will be the subject of future research.

**Remark 4.6** The distinction between the (A) and (B) case has – in essence – already been made in [21]. However, in this paper no attention has been paid to the interactions between these global phenomena and the critical points on the slow manifold or the (non)existence of the higher order intersections.

**Remark 4.7** Kopell and Howard used the existence of the symmetric  $N$ -circuit heteroclinic orbits constructed in [23] to show that the Poincaré map associated to the three-dimensional ODE has an invariant set on which the map acted as a shift map. The heteroclinic orbits constructed in [23] are symmetric connections between one-dimensional manifolds, and thus degenerate from our point of view (see subsection 4.1). However, it is interesting to analyse whether the construction of a horseshoe near an  $N$ -circuit heteroclinic orbit of [23] can also be applied to the heteroclinic orbits found in Theorem 4.2. We will not pursue this subject in this paper.

## 5 The combination of the perturbation analysis and the geometrical approach

In this section we study – as a function of  $P$  – the curves  $\mathcal{C}_{sn}$  (2.18),  $\mathcal{C}_d$  (2.19),  $\mathcal{C}_h$  (3.6) and  $\mathcal{C}_t$  (3.11), the intersections of these curves (that is, the bifurcations of higher co-dimension) and – of course – the changes in the flow of (2.7) caused by crossing of one these curves in the  $(V, W)$ -plane. We only know the position of these curves with an  $O(1)$  accuracy, we must be aware that all the critical values we find for  $P$  in this section are only valid up to  $O(\varepsilon)$ . We will soon see that there are many complicated situations possible, so we will mostly focus on the main themes:  $P = 0$  versus  $P \neq 0$ : the breaking of the hidden symmetry and the application of Theorem 4.2. We will consider some of the other phenomena, but leave their analysis to future research.

It should be noted, however, that in this paper we only pay attention to the characteristics of the flow near  $\cdot$ , and its stable and unstable manifolds,  $W^s(\cdot, \cdot)$  and  $W^u(\cdot, \cdot)$ . To get a more complete picture we should also derive expressions for the curve  $\mathcal{C}_{Hopf}$  – at



which periodic solutions are created/annihilated by a Hopf bifurcation – the curve  $\mathcal{C}_{cn}$  – at which perturbed center points merge – etc. These bifurcations – and others (such as: bifurcation curves related to changes in the stability type of the periodic solution, or to the creation of heteroclinic connections between perturbed saddles and perturbed centers) – have been considered in [8] for a model problem. The analysis of this model problem is much easier: for instance,  $\Delta$  is not bounded and  $(0, z)$  always only changes sign once, thus  $\mathcal{C}_d$  and  $\mathcal{C}_t$  do not exist in this model problem. The curves  $\mathcal{C}_{Hopf}$  and  $\mathcal{C}_{cn}$  have been derived for the cubic,  $P = 0$ , Ginzburg-Landau case in [6]. In principle, these phenomena can also be analysed for (2.7): as for the model problem in [8], a combination of the geometrical approach and the ‘tools’ developed in section 3 must be sufficient. However, we decided to focus on the solutions to (2.7) which correspond to traveling localised structures which connect stable patterns at  $\pm\infty$  in (2.1). Thus, we only need to consider the flow of (2.7) near  $\infty \cup W^s(\infty) \cup W^u(-\infty)$  and only to study the influence of the curves  $\mathcal{C}_{sn}$ ,  $\mathcal{C}_d$ ,  $\mathcal{C}_h$  and  $\mathcal{C}_t$ .

Since we will derive a number of critical values of  $P$ , corresponding to structural changes in the parameter plane  $(W, V)$ , and thus in the flow induced by (2.7) we recall the definitions of  $P$ ,  $W$  and  $V$ :

$$P = -\frac{q}{b-a}, \quad W = \frac{\hat{w} + a}{b-a}, \quad V = \frac{\hat{v}}{b-a},$$

where  $\varepsilon a$ ,  $\varepsilon b$  and  $\varepsilon q$  are the (small) imaginary parts of the coefficients of the perturbed Ginzburg-Landau equation (2.1) and  $v = \varepsilon \hat{v}$ ,  $w = \hat{w}$  the (slow) wave speed and frequency of its solutions  $u$  (2.3). Thus, a critical value of  $P$  corresponds to a critical combination of the imaginary parts of the coefficients in front of the terms  $u_{xx}$ ,  $|u|^2 u$  and  $|u|^4 u$  in the perturbed Ginzburg-Landau equation.

## 5.1 The bifurcation curves $\mathcal{C}_{sn}$ , $\mathcal{C}_d$ , $\mathcal{C}_h$ and $\mathcal{C}_t$

First, we note that there is an useful symmetry in (2.7) (and in (2.8)):

$$(5.1) \quad x \rightarrow x, \quad y \rightarrow -y, \quad z \rightarrow -z, \quad t \rightarrow -t \quad \text{and} \quad V \rightarrow -V.$$

Thus, we see that we can avoid the ‘ $\pm$ ’ in (2.18), (3.6) and (3.11) by considering the system in the  $(W, V^2)$  parameter plane.

The curves  $\mathcal{C}_{sn}$ ,  $\mathcal{C}_h$  and  $\mathcal{C}_t$  are bounded. The boundaries can be obtained by taking  $X = 1$  or  $X = \frac{2}{3}$ . We observe:

$$(5.2) \quad \begin{aligned} D_{11} &\stackrel{\text{def}}{=} (W_{sn}(1), V_{sn}^2(1)) = (W_h(1), V_h^2(1)) = (-(1+P), 0), \\ D_{12} &\stackrel{\text{def}}{=} (W_t(1), V_t^2(1)) = \left(-\frac{1}{15}(5+3P), 0\right). \end{aligned}$$

Thus:  $X \rightarrow 1$  yields  $V \rightarrow 0$ . This is not completely surprising: symmetry (5.1) becomes symmetry (4.1) for the total flow induced by (2.7), or (2.8), if  $V = 0$  (see subsection 4.1). Furthermore,  $z \rightarrow 0$  as  $X \rightarrow 1$  (2.11) and  $\{z = 0\}$  is a plane of symmetry for  $V = 0$ . We (again) refer to [16], [5] and [6] for more details on the relation  $z = 0 \leftrightarrow V = 0$  in the

cubic Ginzburg-Landau equation ( $P = 0$ ). At the other boundary we have:

$$(5.3) \quad D_d \stackrel{\text{def}}{=} (W_{sn}(\frac{2}{3}), V_{sn}^2(\frac{2}{3})) = (W_h(\frac{2}{3}), V_h^2(\frac{2}{3})) \\ = (W_t(\frac{2}{3}), V_t^2(\frac{2}{3})) = (-\frac{4}{3}(1+P), \frac{4}{27}(3+4P)^2) \in \mathcal{C}_d,$$

thus, the behaviour near the degenerate planes  $\{z = \pm\sqrt{\frac{4}{27}}\}$  indeed seems to be quite complicated. Moreover, we can check that all curves are tangent to each other and to  $\mathcal{C}_d$  at  $X = \frac{2}{3}$ .

We now consider only some of the properties of  $\mathcal{C}_{sn}$ ,  $\mathcal{C}_h$  and  $\mathcal{C}_t$  as function of a decreasing  $P$ . As observed in the introduction of this section: all critical values of  $P$  given below are only known up to  $O(\varepsilon)$  corrections. We only pay attention to the qualitative changes in the curves, not to their changes in magnitude. We refer to the next subsection for plots of (parts of)  $\mathcal{C}_{sn}$ ,  $\mathcal{C}_h$  and  $\mathcal{C}_t$  (Figures 5, 6, 7 and 8).

Saddle-node bifurcation curve  $\mathcal{C}_{sn}$  develops a cusp as  $P$  decreases through  $-\frac{1}{2}$ :  $\frac{d}{dX}V_{sn} = \frac{d}{dX}W_{sn} = 0$  for  $X = (4P - 1)/(6P)$ ; this value of  $X$  must be  $\in (\frac{2}{3}, 1)$ , thus we conclude that  $\mathcal{C}_{sn}$  is ‘cusped’ for  $P < -\frac{1}{2}$  (see Figure 6). In the next subsection we will see that the creation of this cusp – as  $P$  decreases from 0 – yields heteroclinic solutions of type (B) in Theorem 4.2.

Homoclinic bifurcation curve  $\mathcal{C}_h$  has a somewhat more complicated behaviour, although it is not cusped. For  $P > -\frac{5}{8}$  there are no points on  $\mathcal{C}_h$  with either  $\frac{d}{dX}W_h = 0$  or  $\frac{d}{dX}V_h^2 = 0$  (Figure 5). This changes at  $P = -\frac{5}{8}$  (Figure 7). At  $P = -\frac{3}{4}$ ,  $\mathcal{C}_h$  becomes tangent to  $\{V = 0\}$  (Figure 8). This minimum on the axis only disappears as  $P$  decreases through  $-\frac{5}{6}$ . In the next subsection we will see that the disappearance of this minimum is directly related to the disappearance of the type (B) heteroclinic orbits. However, the most interesting behaviour of  $\mathcal{C}_h$  occurs in the  $P$ -interval  $[-\frac{10}{13}, -\frac{49}{64}]$  since  $\mathcal{C}_h$  has self-intersections for these  $P$  values. This means that there are parameter combinations  $(W, V^2)$  such that there are two homoclinic bifurcations – near different  $z$ -planes – occurring in (2.7). These two bifurcations merge – that is, appear near the same  $z$ -plane ( $\{z=0\}$ !) – if  $P \rightarrow -\frac{10}{13}$  (see Figure 8 for a plot of  $\mathcal{C}_h$  before and after this interval of self-intersections).

The curve  $\mathcal{C}_t$  is also cusped for  $P \in (-\frac{15}{2}, -\frac{15}{32})$ . However, this cusp does not have much influence on the flow of (2.7) since it is always outside the parabola  $\mathcal{C}_d$  in a region where there are no critical points on  $\cdot$ . So, inside a certain area created by the cusp,  $\Delta_{\text{rgl}}(0, z)$  can have five zeros, but none of them can induce a heteroclinic orbit (for this reason the cusp of  $\mathcal{C}_t$  does not appear in Figures 5, 6, 7, 8). Related to the cusp is a minimum on  $\{V = 0\}$  which exists for  $P \in (-\frac{15}{2}, -\frac{3}{4})$  (Figure 8). There are also self-intersections for  $P \in (-\frac{15}{2}, -\frac{2085}{4598} - \frac{675}{4598}\sqrt{5})$  – where the latter number is  $\approx -0.781\dots$  (Figure 8). We will see in subsection 5.2 that the creation of this self-intersection immediately yields the existence of the case (A) heteroclinic solutions described in Theorem 4.2. These self-intersections take place in a region without critical points for  $P < -\frac{60}{53}$ .

## 5.2 The bifurcations

We found in the above subsection that the structure of the curves  $\mathcal{C}_{sn}$ ,  $\mathcal{C}_h$  and  $\mathcal{C}_t$  changes considerably as function of  $P$ . However, much more important to the behaviour of the flow induced by (2.7) are changes in the configuration of all 4 curves –  $\mathcal{C}_{sn}$ ,  $\mathcal{C}_d$ ,  $\mathcal{C}_h$  and  $\mathcal{C}_t$  – in the  $(W, V^2)$ -plane as function of  $P$ . New configurations yield new regions in the  $(W, V^2)$ -plane bounded by the bifurcation curves. For instance, we will see that the region of type (A) heteroclinic connections disappears (temporarily) as  $P$  decreases through  $-\frac{3}{5} + O(\varepsilon)$  since the minimum of  $\mathcal{C}_d$  passes through the  $X = 1$  endpoint of  $\mathcal{C}_{sn}$  and  $\mathcal{C}_h$  on the  $\{V = 0\}$ -axis,  $D_{11}$  – see (2.19) and (5.2). The characteristics of the flow of (2.7) – near  $\cup W^s(\cdot) \cup W^u(\cdot)$  – in a certain region in  $(W, V^2, P)$ -space do not change as long as the parameter combinations remain bounded away from the bifurcation curves/surfaces.

First, we formulate the main theorems of this section. We refer in the formulation of these theorems to ‘type (A)’ and ‘type (B)’ heteroclinic connections. These characterizations are presented as case (A) or (B) in subsection 4.2 and Theorem 4.2.

**Theorem 5.1** *The non-symmetric co-dimension 2 homoclinic bifurcations only appear for  $P = 0$ . Thus, heteroclinic orbits of the Bekki & Nozaki type only exist for  $P = 0$ . There exist homoclinic orbits to a critical point on  $\Sigma$ , for  $(W, V) \in \mathcal{C}_h(+O(\varepsilon))$ , for all  $P \neq 0$ .*

This theorem is but a reformulation of the main results of subsection 4.1. Note that it is argued at the end of subsection 4.1 (by [23] and [5]) that there will be symmetric (4.1) co-dimension 2 homoclinic bifurcations in the special case  $V = 0$ .

**Theorem 5.2** *Structurally stable (and unique) heteroclinic orbits of type (A) connecting two (perturbed) saddles on  $\Sigma$ , exist in open regions of the  $(V, W)$  parameter plane for  $P > -\frac{3}{5} + O(\varepsilon)$  and  $P < P_A + O(\varepsilon)$  where  $P_A = -\frac{215}{369} - \frac{(15055)5^{\frac{1}{3}}}{1476(-1050233+76014\sqrt{309})^{\frac{1}{3}}} + \frac{5^{\frac{2}{3}}(-1050233+76014\sqrt{309})^{\frac{1}{3}}}{1476} \approx -0.716\dots$*

**Theorem 5.3** *There exist countably many structurally stable multi-circuit heteroclinic orbits of type (B) in open regions of the  $(V, W)$  parameter plane for  $-\frac{15}{11} + O(\varepsilon) < P < -\frac{1}{2} + O(\varepsilon)$ .*

Thus, there are two  $P$ -intervals  $(-\frac{3}{5}, -\frac{1}{2})$  and  $(-\frac{15}{11}, P_A)$  – where type (A) and (B) heteroclinic solutions exist simultaneously. In the former interval the corresponding  $(V, W)$ -regions do not intersect, in the latter interval there are two or even three zeros of  $\Delta_{rgl}(0, z)$  between two saddles on  $\Sigma$ , in certain regions in the  $(V, W)$ -plane: the type (A) and (B) heteroclinic solutions exist for the same choices of  $V$  and  $W$  and are connections between the same perturbed saddles.

We remark that the cubic Ginzburg-Landau case,  $P = 0$ , does not appear in Theorem 5.3 and conclude:

**Corollary 5.4** *Adding a small quintic term  $\varepsilon\gamma|u|^4u$  to the cubic Ginzburg-Landau equation breaks the hidden symmetry and creates families of traveling multi-circuit solutions to (2.1) which do not exist for  $\gamma = 0$ .*

It is fairly easy to obtain a picture of the  $N$ -circuit solutions as solutions of the PDE (1.1), or (2.1), (2.2). The 0-circuit solution, that is, the part of , between the two (perturbed) saddles (see subsection 4.2) corresponds to a localised structure which ‘smoothly’ connects the two periodic patterns – corresponding to  $S_1$  and  $S_2$  at  $x = \pm\infty$ . This can be seen by noticing that  $x$  and  $t$  in (2.7) correspond to  $|u|$  and  $x + vt$  in the PDE context (see section 2). Thus,  $|u|$  decreases or increases slowly and monotonically for the localised structure corresponding to the 0-circuit orbit. These solutions are called weak shocks in [18]. A 1-circuit orbit remains close to , except for one ‘detour’ through the fast field. For the corresponding localised structure this means that there is the same monotonic and slow behaviour as for the 0-circuit orbit except for one fast ‘hole’ where  $|u|$  jumps away and returns. The localised structures which correspond to an  $N$ -circuit heteroclinic orbit have  $N$  of these fast ‘holes’ or ‘jumps’ in  $|u|$ . Notice also that the multi-circuit or multi-jump solutions are only close to solutions of the cubic Ginzburg-Landau equation for finite intervals of time/space: there are no solutions to the cubic equation which are  $O(\varepsilon)$  close to a multi-circuit/jump solution for all  $x$  and  $t$ .

The proofs of Theorems 5.2 and 5.3 should consist of a detailed study of all structurally different configurations of  $\mathcal{C}_{sn}$ ,  $\mathcal{C}_d$ ,  $\mathcal{C}_h$  and  $\mathcal{C}_t$  as  $P$  is varied. For every configuration we should check the (number of) critical points on , , the number of zeros of  $\Delta$ ,  $\gamma_l(0, z)$ , the relative positions – with respect to the  $z$  direction – of these points and the direction of the (slow) flow on , . Based on this, we can see in which regions of the  $(W, V^2)$ -plane Theorem 4.2 can be applied. In a sense this is a straightforward – but very cumbersome – job. Therefore, we will mostly focus on the following five critical cases:  $P$  near 0,  $-\frac{1}{2}$ ,  $-\frac{3}{5}$ ,  $P_A$  and  $-\frac{15}{11}$  and make some short remarks on the bifurcations which occur for other values of  $P$ .

**$P = 0$ ,  $P$  near 0 and  $P$  positive.**

It is easy to check that  $\Delta$ ,  $\gamma_l(0, z)$  (3.9) always has a unique zero outside the  $\mathcal{C}_d$  parabola for  $|W|$  large enough and has no zeros inside this parabola for  $V$  large enough. The opposite is true for the (perturbed) saddles on , (2.17): they do not exist outside the  $\mathcal{C}_d$  parabola for  $|W|$  large enough and there is a unique critical point inside this parabola for  $V$  large enough. Thus, independent of  $P$ , we can only expect interesting behaviour in regions of the  $(W, V^2)$  in the neighbourhood of the bounded curves  $\mathcal{C}_{sn}$ ,  $\mathcal{C}_h$  and  $\mathcal{C}_t$ . We have plotted  $\mathcal{C}_{sn} = \mathcal{C}_h$ ,  $\mathcal{C}_d$  and  $\mathcal{C}_t$  for  $P = 0$  in Figure 5: if we fix  $V$  at a value below the  $V$ -coordinate of the mutual  $X = \frac{2}{3}$  boundary,  $D_d$  (5.3), we observe for increasing  $W$ : a saddle-node bifurcation, immediately ( $O(\varepsilon^2)$ , remark 4.1) followed by the co-dimension 2 homoclinic bifurcation at which a Bekki & Nozaki solution exists (subsection 4.1), thus entering a region bounded by  $\mathcal{C}_h$ ,  $\mathcal{C}_d$  and  $\{V = 0\}$  in which  $\Delta$ ,  $\gamma_l(0, z)$  has one zero between the two critical points on , . By a simple check we find that this is a case (A) situation (Theorem 4.2): there is one unique heteroclinic connection  $\gamma_{\text{het}}(t)$ . Since this is the only area in the  $(W, V^2)$  plane in which there is more than one critical point of perturbed saddle type, there is no need to search for other heteroclinic connections between (perturbed)

saddles (Figure 5).

For  $P > 0$  there is essentially only one major difference:  $\mathcal{C}_{sn}$  and  $\mathcal{C}_h$  become disconnected –  $\mathcal{C}_{sn}$  is to the left of  $\mathcal{C}_h$  – such that the type (A) orbits  $\gamma_{\text{het}}(t)$  are now created by an ordinary co-dimension 1 homoclinic bifurcation – subsection 4.1 – if  $W$  increases and  $V$  is kept fixed. The structures of  $\mathcal{C}_{sn}, \mathcal{C}_d, \mathcal{C}_h, \mathcal{C}_t$  and their intersections remain topologically the same for all  $P > 0$ . If  $P$  becomes negative there is one additional phenomenon which eventually leads to the disappearance of the type (A) region: again  $\mathcal{C}_{sn}$  is to the left of  $\mathcal{C}_h$ , but now there is an intersection of  $\mathcal{C}_h$  and  $\mathcal{C}_d$  below  $D_d$  (this intersection approaches  $D_d$  as  $P \uparrow 0$ ). Thus, the intersection  $\mathcal{C}_h \cap \mathcal{C}_d$ , and not  $D_d$ , is the ‘top’ of the type (A) region bounded by  $\mathcal{C}_h, \mathcal{C}_d$  and  $\{V = 0\}$ . This point comes down to the  $V$ -axis as  $P$  decreases. Note that the  $\mathcal{C}_{sn}(P)$  and  $\mathcal{C}_h(P)$  surfaces are tangent at  $P$  and do not really intersect (non-transversely), as was already explained in subsection 4.1.

**$P$  near  $-\frac{1}{2}$ : a cusp on  $\mathcal{C}_{sn}$ .**

This cusp is created as  $P$  decreases through  $-\frac{1}{2}$ . Above  $P = -\frac{1}{2}$   $\mathcal{C}_{sn}$  has no interior extrema, this has changed dramatically as  $P < -\frac{1}{2}$ : coming from  $D_d$   $\mathcal{C}_{sn}$  first has a minimum on the  $V$ -axis, then intersects  $\mathcal{C}_h$  and returns to this axis – as  $X \rightarrow 1$  – by the cusp (see Figure 6). Thus, the cusp created two ‘new’ regions in the  $(W, V^2)$  plane: above or below  $\mathcal{C}_h$ , inside the cusp (that is, in the region bounded by the cusped part of  $\mathcal{C}_{sn}$  and  $\{V = 0\}$ , Figure 6,  $P = -0.55$ ). Note that the cusp takes a piece from the type (A) region described above. So, entering the inside of the cusp from the type (A) region yields the creation of two new perturbed saddles on  $, :$  although this might influence the behaviour of  $\gamma_{\text{het}}(t)$  for  $t \rightarrow \pm\infty$  it does not change the type of the heteroclinic connection. However, if one again crosses  $\mathcal{C}_h$  inside this cusp (Figure 6), then the system is in the situation as described by Corollary 4.3: the type (A) situation changes into a type (B) situation: countably infinitely multi-circuit heteroclinic solutions exist in the (initially tiny) region inside the cusp, bounded by  $\mathcal{C}_{sn}, \mathcal{C}_h$  and  $\{V = 0\}$ . This yields the first critical value of  $P$  given in Theorem 5.3.

**$P$  approaches  $-\frac{3}{5}$ .**

As  $P$  decreases further both the intersection  $\mathcal{C}_h \cap \mathcal{C}_d$  – the top of the type (A) region – and the endpoints of  $\mathcal{C}_{sn}$  and  $\mathcal{C}_h$  –  $(-1 - P, 0)$  (5.2) – approach the minimum of  $\mathcal{C}_d$  –  $(-\frac{2}{3} - \frac{4}{9}P, 0)$ . In Figure 6 we plotted  $\mathcal{C}_{sn}$  and  $\mathcal{C}_h$  for  $P = -0.55, -0.57$  – the cusp passes through  $\mathcal{C}_d$  at  $P = -\frac{9}{16}$  – and the critical value  $-\frac{3}{5}$  at which these three points have merged. Thus, the region of type (A) heteroclinic orbits disappears as  $P \downarrow -\frac{3}{5}$ . As a consequence, there are no type (A) heteroclinic orbits as  $P$  has decreased below  $-\frac{3}{5}$  (Theorem 5.2). The type (B) region has grown, at  $P = -\frac{3}{5}$  it is bounded by  $\mathcal{C}_{sn}, \mathcal{C}_h$  and  $\{V = 0\}$ , inside the cusp (Figure 6).

**$P$  near  $P_A$ : the influence of  $\mathcal{C}_t$ .**

So far,  $\mathcal{C}_t$  did not appear in or near regions where Theorem 4.2 could be applied. This changes as the point  $D_{h-t}$  of tangent intersection of  $\mathcal{C}_h$  and  $\mathcal{C}_t$  – which exists at  $X = (5 + 24P)/(18P)$  for  $P \in (-\frac{5}{6}, -\frac{5}{12})$  – comes down to  $\{V = 0\}$ . In Figure 7 we plotted the relevant parts of  $\mathcal{C}_{sn}, \mathcal{C}_d, \mathcal{C}_h$  and  $\mathcal{C}_t$  and the points  $D_{11}, D_d$  and  $D_{h-t}$  for  $P = -0.67$ . Note the structural differences with the cubic Ginzburg-Landau case  $P = 0$  (Figure 5). One

can in essence apply the same arguments as for the intersections of  $\mathcal{C}_{sn}$  and  $\mathcal{C}_h$  (subsection 4.1) to explain that  $\mathcal{C}_h$  and  $\mathcal{C}_t$  must intersect non-transversely:  $\mathcal{C}_h$  ‘needs’ at least one zero of  $\Delta, r_{gl}(0, z)$  (again, a transversal intersection can occur if the bifurcations take place at different values of  $X$ , see Figure 8,  $P = -0.79$ ). At a tangent intersection, the two zeros of  $\Delta, r_{gl}(0, z)$  are created  $O(\varepsilon)$  near the  $z$ -coordinate of a critical point on  $\cdot$ . The co-dimension 2 point  $D_{h-t}$  passes through the curve  $\mathcal{C}_{sn}$  at the value  $P_A$  given in Theorem 5.2. Here, we do not study the details of this co-dimension 3 phenomenon, but only consider the effect of it as  $P < P_A$ : a new region bounded by  $\mathcal{C}_{sn}, \mathcal{C}_h$  and  $\mathcal{C}_t$  – with  $D_{h-t}$  as ‘tip’ where  $W$  is at its maximum (Figure 8). Inside this region, there are three critical points on  $\cdot$ , and two zeros of  $\Delta, r_{gl}$ ; these two intersections of  $W^s(\cdot)$  and  $W^u(\cdot)$  are between two of the three perturbed saddles. Thus, inside this new region Theorem 4.2 can be applied both for case (A) and for case (B): there exists two 1-circuit heteroclinic orbits  $\gamma_{\text{het}}(t)$  – one for each zero of  $\Delta, r_{gl}$  – and one family of type (B) multi-circuit solutions. The type (A) heteroclinic solutions have returned (Theorem 5.2), but are now coupled to the type (B) orbits. Note that  $D_{h-t}$  passes through  $\mathcal{C}_d$  shortly below  $P = P_A$  (Figure 8), however, this bifurcation does not influence the type (A) and (B) heteroclinic orbits.

**Following  $D_d$  as  $P$  decreases further.**

As we said at the beginning of this proof of Theorems 5.2 and 5.3 (and at the beginning of this section): there are many interesting phenomena which won’t be studied in detail. However, we can get an impression of some of them by considering the structure of the bifurcation curves near  $D_d$  as function of  $P$ . At  $P = -\frac{3}{4}$ ,  $D_d \in \{V = 0\}$  (see Figure 8): a number of ‘new’ regions are created as  $P$  becomes smaller than  $-\frac{3}{4}$  since both  $\mathcal{C}_h$  and  $\mathcal{C}_t$  now have a minimum on  $\{V = 0\}$  – the former to the right of the minimum of  $\mathcal{C}_d$ , the latter to the left (see Figure 8,  $P = -0.79$ ). The most interesting new region is bounded  $\mathcal{C}_d, \mathcal{C}_h$  and  $\{V = 0\}$  – with the minima of  $\mathcal{C}_d$  and  $\mathcal{C}_h$  as left/right-‘tips’: there are three zeros of  $\Delta, r_{gl}$  all between two critical points on  $\cdot$ . Thus, for choices of  $(V, W)$  in this region Theorem 4.2 can be applied three times, once for case (B) and twice for case (A). This region will grow and only disappear at  $P = -\frac{15}{11}$ . However, before  $P$  reaches that value much more has happened: first we pass through the region  $[-\frac{10}{13}, -\frac{49}{64}] \approx [-0.769\dots, -0.765\dots]$  where  $\mathcal{C}_h$  has self-intersections (subsection 5.1): many bifurcations occur, but we do not study these here. Then,  $D_d$  passes through  $\mathcal{C}_t$  – at  $P = -\frac{2085}{4598} - \frac{675}{4598}\sqrt{5} \approx -0.781\dots$  – thereby creating a self-intersection of  $\mathcal{C}_t$  (subsection 5.1) and a new region above  $\mathcal{C}_t$ , bounded by  $\mathcal{C}_d, \mathcal{C}_{sn}$  and  $\mathcal{C}_t$  with  $D_d$  as top (see Figure 8,  $P = -0.79$ ). In this region there is one (A) type zero of  $\Delta, r_{gl}$  between two critical points on  $\cdot$ . Thus, the ‘isolated’ type (A)  $\gamma_{\text{het}}(t)$  has reappeared. This region will grow as  $P$  decreases further and will never disappear. Moreover, the  $\mathcal{C}_t$  boundary will eventually – at  $P = -\frac{15}{11}$  – be replaced by  $\{V = 0\}$ ). This concludes the proof of Theorem 5.2.  $\square$

**$P$  near  $-\frac{15}{11}$ : the type (B) heteroclinic orbits disappear.**

The type (B) heteroclinic orbits only exist in (sub)regions of the region to the right and outside the  $\mathcal{C}_d$  parabola and below  $\mathcal{C}_t$  (and, of course, above  $\{V = 0\}$ ). As long as  $P > -\frac{5}{6}$  this region has  $\mathcal{C}_h$  as fourth boundary to the right (see Figure 8). However, as  $P$  decreases through  $-\frac{5}{6}$ , the (tangent) intersection of  $\mathcal{C}_h$  and  $\mathcal{C}_t$ ,  $D_{h-t}$ , merges with the  $X = 1$  end-points of these curves,  $D_{11}, D_{12}$  (5.2), and  $\mathcal{C}_h$  becomes a curve above  $\mathcal{C}_t$ . What remains is a region (bounded by  $\mathcal{C}_d, \mathcal{C}_t$  and  $\{V = 0\}$ ) which was created at  $P = -\frac{3}{4}$  (see above):

in it, two type (A) heteroclinic orbits coexist with a type (B) family of heteroclinic orbits. This region shrinks as  $P$  decreases further: its three tips coalesce at  $P = -\frac{15}{11}$ . Thus, the type (B) heteroclinic orbits disappear at  $P = -\frac{15}{11}$  and Theorem 5.3 has been proved.  $\square$

**$P$  below  $-\frac{15}{11}$ .**

As  $P$  decreases further not much happens. The isolated type (A) region keeps on growing. The cusp, the self-intersection and the minimum of  $\mathcal{C}_t$  exist as long as  $P > -\frac{15}{2}$ , thus ‘keeping alive’ (tiny) regions where  $\Delta_{, ryl}(0, z)$  can have up to five zeros. However, there are no critical points on  $\mathcal{C}_t$  in these regions. Thus, the ‘fate’ of the solutions corresponding to these intersections is coupled to the behaviour of  $\mathcal{C}_t$  outside the  $O(\varepsilon)$  neighbourhood of the curve of unperturbed saddle points (see Remark 3.1). The structures of  $\mathcal{C}_{sn}$ ,  $\mathcal{C}_d$ ,  $\mathcal{C}_h$ ,  $\mathcal{C}_t$  and their intersections remain topologically the same for all  $P < -\frac{15}{2}$ .

## 6 Discussion

The existence of the hidden symmetry can have far-reaching consequences for the study of pattern formation at near-critical conditions by the (cubic) Ginzburg-Landau equation. As in [26], [27] and [30] we have shown that the higher order nonlinear effects modeled by the small quintic term in (1.1) break this hidden symmetry. Thus, the hidden symmetry is a property of the cubic Ginzburg-Landau equation itself and is not related to properties of the underlying system on which the Ginzburg-Landau equation is based. However, this means that one should be careful in using the cubic Ginzburg-Landau equation – especially when one is interested in traveling waves – since one introduces a non-generic phenomenon into the equation by neglecting the higher order terms. Furthermore, we have shown that these higher order terms do have an essential influence on the structure of the solutions: the ‘multi-jump’ heteroclinic solutions found in this paper do not exist in the cubic case.

So, one can say that the above observations – in some sense – justify the use of Ginzburg-Landau equations with quintic terms in the theoretical study of traveling patterns such as those observed in [2] (see [29] for references). However, from a derivational point of view the higher order nonlinearities should be small compared to the cubic term, while in most studies of ‘extended’ Ginzburg-Landau equations all terms are considered to be of the same magnitude (we again refer to [29] for a list of references, see also [9], [17], [19]). This ‘gap’ between, on one side, the Ginzburg-Landau equation as modulation equation derived from an underlying system and, on the other side, as model equation has, of course, been noticed by many authors (see also [22] for a more general discussion). The existence of a co-dimension 2 phenomenon in the cubic equation once more indicates that this gap should, at least, be the subject of further investigations. A first step has already been made in [12] and [7], but there the authors had to assume that the real part of the coefficient of the cubic term –  $\beta$  in (1.1) – is small compared to the other terms in the cubic equation.

After section 2 we did not pay much attention to the nonlinear Schrödinger limit. This was motivated by the observation that this limit induces an ODE reduction which can be seen as subcase of the ODE reduction of the real Ginzburg-Landau limit (compare (2.8) to (2.7), moreover,  $V$  does only have an  $O(\varepsilon)$  influence in the nonlinear Schrödinger limit (2.8) – section 3). However, the nonlinear Schrödinger subcase,  $V = 0$ , is strongly related

to the degenerations in the  $\{z = 0\}$ -plane which we avoided as much as possible in this paper (except for a short discussion in subsection 4.1). Thus, it is a natural next step to analyse the degenerations of the ODE reductions – at  $z = 0$  and  $z = \pm\sqrt{\frac{4}{27}}$  – in the context of the nonlinear Schrödinger limit. This can be done by the methods developed in this paper combined with the use of the extra symmetries in this case (subsection 4.1, see also [23], [16] and [5]). Furthermore, one must be able to use the ideas presented in [20] to study , – and curves near it – when it is not close to the curve of unperturbed saddles (at least in a special region in the parameter plane). The extra information obtained from this ‘slow manifold approach’ can then be compared with the results of [30].

The slow manifold approach enabled us to find large families of localised solutions which exist in open regions of the parameter space, that is  $r \in \mathbf{R}$ ,  $\alpha, \beta, \gamma \in \mathbf{C}$  in (1.1) and  $v, w$  from (2.3). These solutions consist of distinguished ‘slow’ and ‘fast’ parts, therefore, it is unlikely that an explicit formula can be obtained for any of these solutions. It’s probably for this reason that none of these structurally stable heteroclinic orbits – not even the type (A) orbits in the cubic Ginzburg-Landau case – have been found in [29] and [24], where the attention is focused on exact solutions. Moreover, the solutions found in this paper are not close to a solution of the integrable limit for all  $\xi (= x + vt)$  and therefore cannot be found by a more straightforward perturbation analysis (as for instance in [29], [30]).

In this paper we did not pay any attention to the stability of the constructed localised structures as solutions of the partial differential equation (1.1). Of course this is a necessary next step. This can be done by numerical simulations combined with arguments obtained by perturbation analysis – see [29], [27], [26]. However, there also exist mathematical methods especially developed to study rigorously the stability of heteroclinic solutions which are related to a slow manifold. The results of [18] indicate that – under some conditions – the ‘0-jump’ solutions are stable as ‘weak shocks’ in the PDE. These solutions correspond to the 0-circuit heteroclinic orbits on , between the saddles  $S$  and  $\hat{S}$  (subsection 4.2).



## References

- [1] N. Bekki and B. Nozaki (1985) Formations of spatial patterns and holes in the generalized Ginzburg-Landau equation, *Phys. Lett.* **110A** 133-135.
- [2] D. Bensimon, P. Kolodner, C.M. Surko, H. Williams and V. Croquette (1990) Competing and coexisting dynamical states of traveling-wave convection in an annulus, *J. Fluid Mech.* **217** 441-467.
- [3] P. Bollerman, A. van Harten and G. Schneider (1995) On the justification of the Ginzburg-Landau approximation, pp 20-36 in *Nonlinear Dynamics and Pattern Formation in the Natural Environment* (A. Doelman and A. van Harten eds.), Longman, UK, to appear.
- [4] P. Collet and J.P. Eckman (1990) The time-dependent amplitude equation for the Swift-Hohenberg problem, *Comm. Math. Phys.* **132** 139-153.
- [5] A. Doelman (1989) Slow time-periodic solutions of the Ginzburg-Landau equation, *Physica* **40D** 156-172.
- [6] A. Doelman (1993) Traveling waves in the complex Ginzburg-Landau equation, *J. Nonlinear Sc.* **3** 225-266.
- [7] A. Doelman and W. Eckhaus (1991) Periodic and quasi-periodic solutions of degenerate modulation equations, *Physica* **53D** 249-266.
- [8] A. Doelman and P. Holmes (1995) Homoclinic explosions and implosions, to appear in *Proc. Roy. Soc. Lond. A*.
- [9] J. Duan and P. Holmes (1994) Fronts, domain walls and pulses for a generalized Ginzburg-Landau equation, *Proc. Edinburgh Math. Soc.* **38** 77-97.
- [10] W. Eckhaus (1965) *Studies in Nonlinear Stability Theory*, Springer-Verlag.
- [11] W. Eckhaus (1992) On modulation equations of the Ginzburg-Landau type, in *ICIAM 91: Proc. 2nd Int. Conf. Ind. Appl. Math.* (R.E. O'Malley ed.) 83-98.
- [12] W. Eckhaus and G. Iooss (1989) Strong selection or rejection of spatially periodic patterns in degenerate bifurcations, *Physica* **39D** 124-146.
- [13] N. Fenichel (1979) Geometric singular perturbation theory for ordinary differential equations, *J. Diff. Eq.* **31** 53-98.
- [14] A. van Harten (1991) On the validity of Ginzburg-Landau's equation, *J. Nonlinear Sci.* **1**, 397-422.
- [15] L.M. Hocking and K. Stewartson (1972) On the nonlinear response of a marginally unstable plane parallel flow to a two-dimensional disturbance, *Proc. Roy. Soc. Lond. A* **326** 289-313.
- [16] P. Holmes (1986) Spatial structure of time-periodic solutions of the Ginzburg-Landau equation, *Physica* **23D** 84-90.

- [17] C.K.R.T. Jones, T. Kapitula and J. Powell (1990) Nearly real fronts in a Ginzburg-Landau equation, *Proc. Roy. Soc. Edin. A* **116** 193-206.
- [18] T. Kapitula (1991) Stability of weak shocks in  $\lambda - \omega$  systems, *Ind. Univ. Math. J.* **40** 1193-1219.
- [19] T. Kapitula (1995) Singular heteroclinic orbits for degenerate modulation equations, *Physica* **82D** 36-59.
- [20] T. Kapitula and S. Maier-Paafe (1995) Spatial dynamics of time periodic solutions for the Ginzburg-Landau equation, preprint.
- [21] W. Kath (1985) Slowly varying phase planes and boundary layer theory, *Stud. Appl. Math.* **72** 221-239.
- [22] E. Knobloch (1995) Remarks on the use and misuse of the Ginzburg-Landau equation, pp 130-146 in *Nonlinear Dynamics and Pattern Formation in the Natural Environment* (A. Doelman and A. van Harten eds.), Longman, UK, to appear.
- [23] N. Kopell and L.N. Howard (1981) Target patterns and horseshoes from a perturbed central force problem: some temporally periodic solutions to reaction diffusion problems, *Stud. Appl. Math.* **64** 1-56.
- [24] P. Marcq, H. Chaté and R. Conte (1994) Exact solutions of the one-dimensional complex Ginzburg-Landau equation, *Physica* **73D** 305-317.
- [25] B.J. Matkovsky and V. Volpert (1993) Stability of plane wave solutions of complex Ginzburg-Landau equations, *Quart. Appl. Math* **51** 265-281.
- [26] S. Popp, O. Stiller, I. Aranson and L. Kramer (1995) Hole solutions in the 1d complex Ginzburg-Landau equation, to appear in *Physica D*.
- [27] S. Popp, O. Stiller, I. Aranson, A. Weber and L. Kramer (1993) Localised hole solutions and spatiotemporal chaos in the 1D complex Ginzburg-Landau equation, *Phys. Rev. Lett.* **70** 3880-3883.
- [28] C. Robinson (1983) Sustained resonance for a nonlinear system with slowly varying coefficients, *SIAM Math. An.* **14** 847-860.
- [29] W. van Saarloos and P. C. Hohenberg (1992) Fronts, pulses, sources and sinks in generalized complex Ginzburg-Landau equations, *Physica* **56D** 303-367.
- [30] O. Stiller, S. Popp and L. Kramer (1995) From dark solitons in the defocusing nonlinear Schrödinger equation to holes in the complex Ginzburg-Landau equation, to appear in *Physica D*.
- [31] J.T. Stuart and R.C. DiPrima (1978) The Eckhaus and Benjamin-Feir resonance mechanisms, *Proc. Roy. Soc. Lond. A* **362** 27-41.
- [32] S. Wiggins (1988) *Global Bifurcations and Chaos*, Springer-Verlag.
- [33] S. Wiggins (1994) *Normally Hyperbolic Invariant Manifolds in Dynamical Systems*, Springer-Verlag.

## A The derivation of $\Delta\Gamma_{rgl}(0, z)$

First we note that  $x_h(t)$  is even and  $y_h(t) = \dot{x}_h(t)$  is odd as function of  $t$  (2.16). This immediately yields that the terms involving  $Q$  ‘average out’. The same is true for the terms involving  $V$  in the NLS limit. Since  $\frac{2y_h}{x_h^3} = -\frac{d}{dt}\frac{1}{x_h^2}$  we can write (3.7) as

$$(A.1) \quad \Delta,_{rgl}(0, z) = -2 \lim_{L \rightarrow \infty} \int_0^L \left\{ [V y_h^2 + z(W + x_h^2 + P x_h^4) + V \frac{z^2}{x_h^2}] \right. \\ \left. - \frac{z}{x_h^2(L)} [W x_h^2 + x_h^4 + P x_h^6 + V z] \right\} dt.$$

We can now use (2.10) to transform (A.1) into

$$(A.2) \quad \Delta,_{rgl}(0, z) = -2 \lim_{L \rightarrow \infty} \int_0^L \left\{ [V I + W z - \frac{V z^2}{x_h^2(L)}] + [z - V - \frac{W z}{x_h^2(L)}] x_h^2 \right. \\ \left. + [P z + \frac{V}{2} - \frac{z}{x_h^2(L)}] x_h^4 - \frac{P z}{x_h^2(L)} x_h^6 \right\} dt.$$

Next, we introduce  $H(t) = x_h^2(t) - X_s$ :  $\lim_{t \rightarrow \infty} H(t) = 0$ , exponentially fast (2.16). Since the integral cannot grow faster than linear as function of  $L$  we are thus allowed to substitute  $X(= X_s)$  for  $x_h^2(L)$  in (A.2) and observe by (2.10) that all linear terms disappear from (A.2). We now can express  $\Delta$ , as the sum of three convergent integrals:

$$(A.3) \quad \Delta,_{rgl}(0, z) = 2[z + P X z + \frac{W z}{X} + V - V X] I_1^H + 2[2P z + \frac{z}{X} + \frac{V}{2}] I_2^H + \frac{2P z}{X} I_3^H,$$

where

$$I_j^H = \int_0^\infty H^j(t) dt = \sqrt{2}(3X - 2)^{j-1} \int_0^\infty (\tanh^2 s - 1)^j ds$$

for  $j = 1, 2, 3$  (2.16). These integrals can be evaluated explicitly:

$$I_1^H = -\sqrt{2}, \quad I_2^H = \frac{2}{3}\sqrt{2}(3X - 2), \quad I_3^H = -\frac{8}{15}\sqrt{2}(3X - 2)^2.$$

Combining these results with (A.3) and (2.11) yields (3.9).

## Figure captions

Figure 1:

The bounded solutions of the integrable system (2.9) for  $0 < z < \sqrt{\frac{4}{27}}$ .

Figure 2:

The intersection  $\gamma_{\text{int}}(t)$  of  $W^u(\cdot)$  and  $W^s(\cdot)$  as heteroclinic orbit between the perturbed saddle points  $S_1$  and  $S_2$  on  $\Sigma$ .

Figure 3:

The intersection  $\gamma_{\text{int}}(t)$  at the two co-dimension 1 homoclinic bifurcations and at the intermediate co-dimension 2 bifurcation.

Figure 4:

A sketch of the intersections  $\mathcal{P}(\cdot)$  and  $\mathcal{P}^{-1}(\cdot)$  of  $W^u(\cdot)$  and  $W^s(\cdot)$  with  $\{y = 0\}$  and their higher order iterates in case (A) and case (B);  $\gamma_{\text{int}}(t)$ ,  $W^{\text{ss}}(S_1)$ ,  $W^{\text{uu}}(S_1)$ ,  $W^{\text{ss}}(S_2)$  and  $W^{\text{uu}}(S_2)$  have been added as ‘schematic projections’.

Figure 5:

The curves  $\mathcal{C}_{sn} = \mathcal{C}_h$ ,  $\mathcal{C}_d$  and  $\mathcal{C}_t$  and their endpoints  $D_{11}$ ,  $D_{12}$  and  $D_d$  (5.2), (5.3) in the  $(W, V^2)$  plane for  $P = 0$ ; the type (A) heteroclinic connections exist in the region bounded by  $\mathcal{C}_{sn} = \mathcal{C}_h$ ,  $\mathcal{C}_d$  and  $\{V = 0\}$ .

Figure 6:

Parts of the curves  $\mathcal{C}_{sn}$ ,  $\mathcal{C}_h$  and  $\mathcal{C}_d$  for  $P = -0.55$ ,  $-0.57$  and  $-0.60$ .

Figure 7:

The (relevant parts of)  $\mathcal{C}_{sn}$ ,  $\mathcal{C}_d$ ,  $\mathcal{C}_h$  and  $\mathcal{C}_t$  for  $P = -0.67$ . Type (B) multi-circuit heteroclinic orbits exist in the region bounded by  $\mathcal{C}_{sn}$ ,  $\mathcal{C}_h$  and  $\{V = 0\}$ , ‘inside’ the  $\mathcal{C}_{sn}$  cusp.

Figure 8:

The curves  $\mathcal{C}_{sn}$ ,  $\mathcal{C}_d$ ,  $\mathcal{C}_h$  and  $\mathcal{C}_t$  for  $P = -0.75$  and  $-0.79$ .

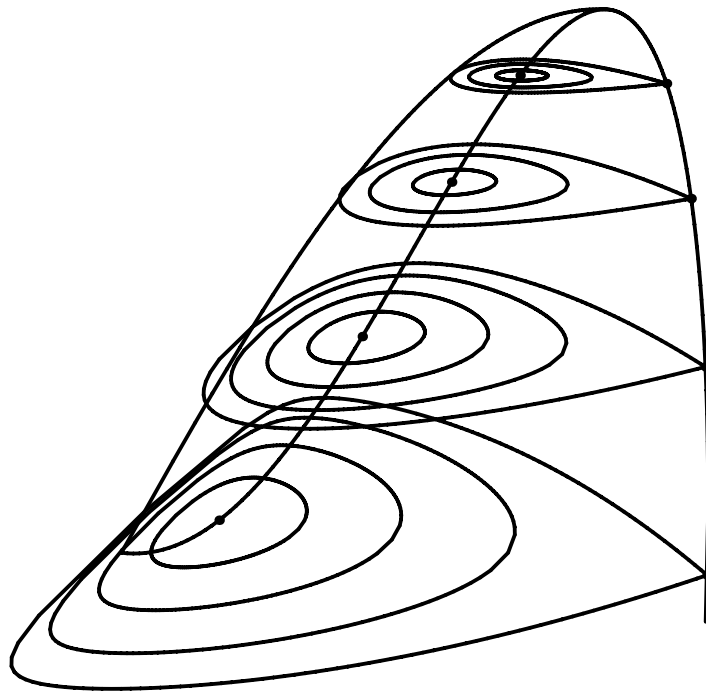


Figure 1:

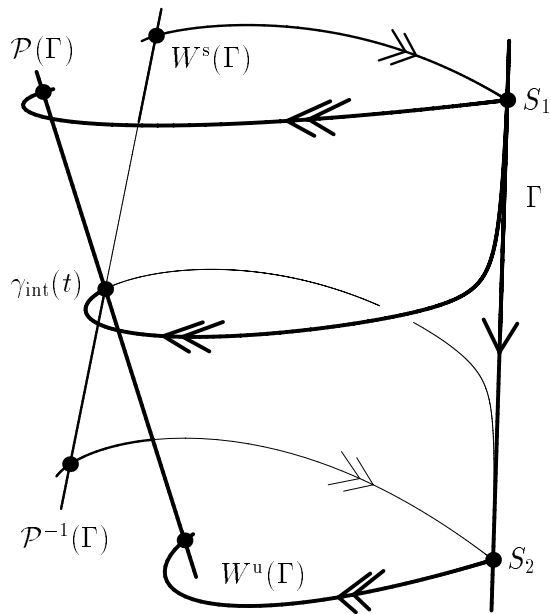


Figure 2:

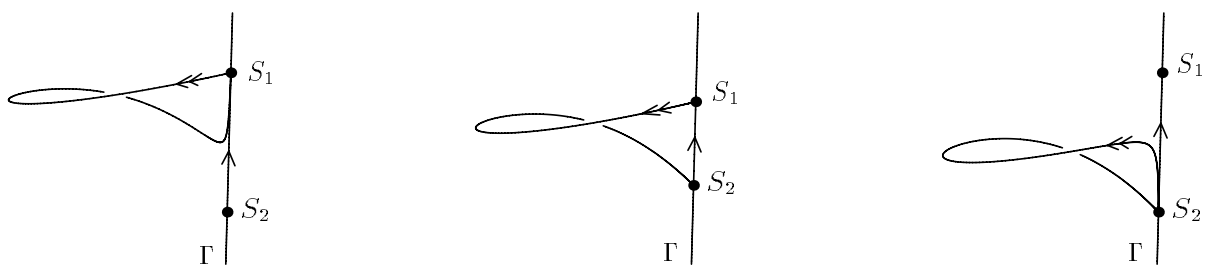


Figure 3:

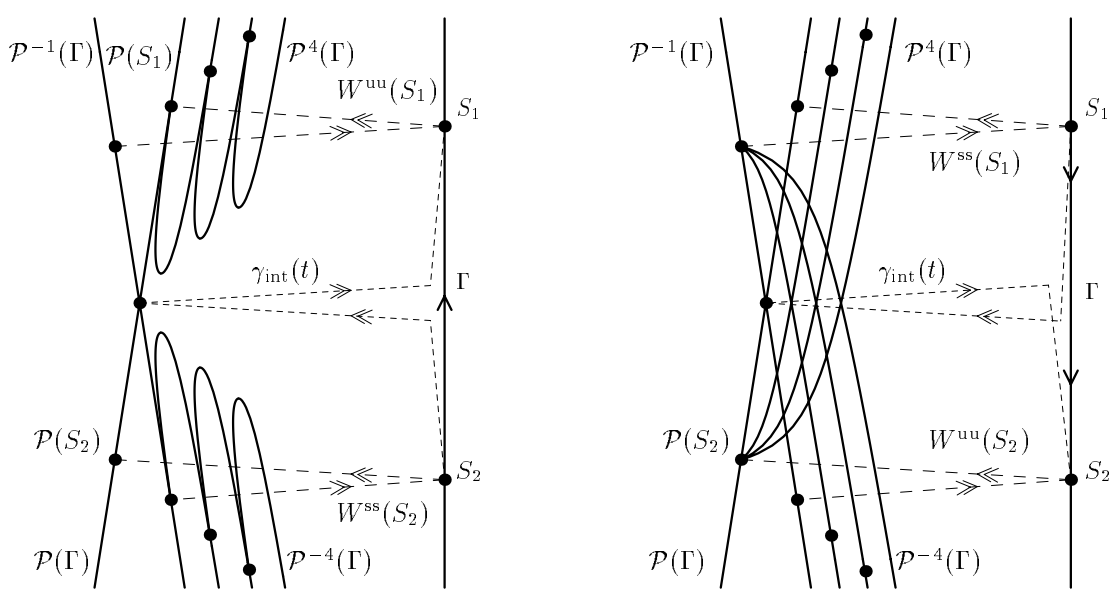


Figure 4:

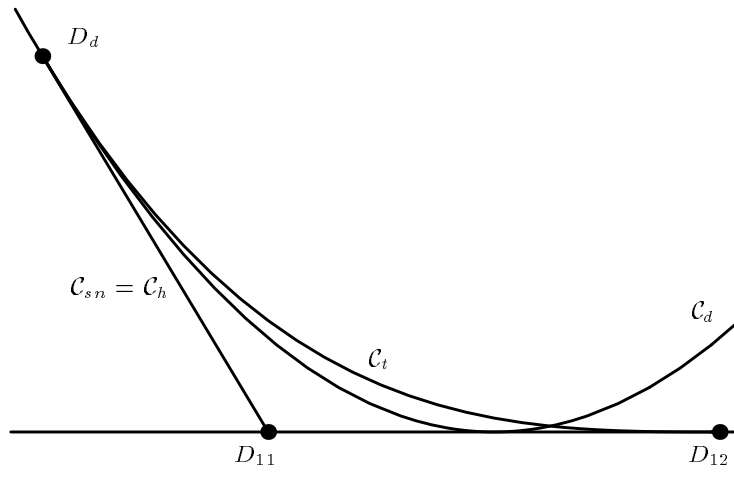


Figure 5:

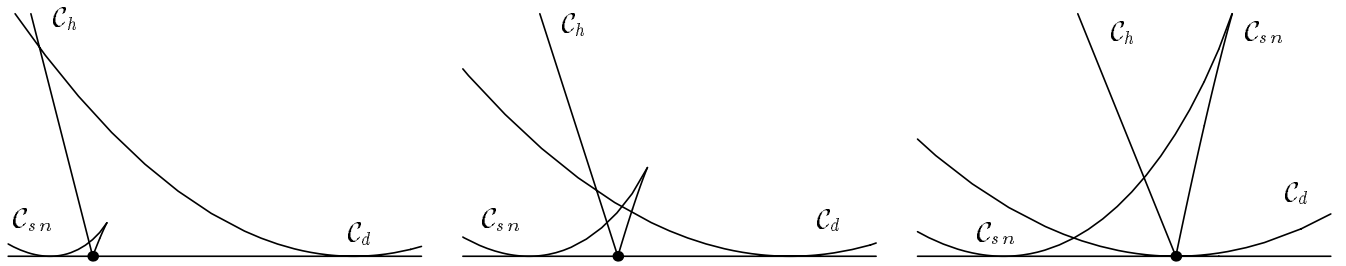


Figure 6:

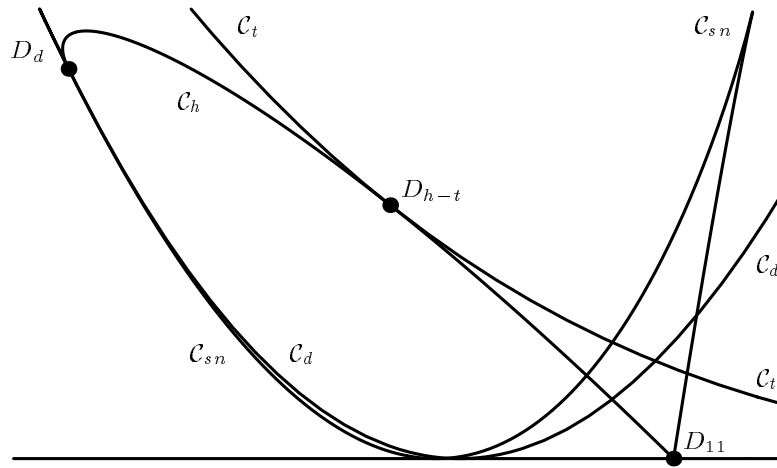


Figure 7:

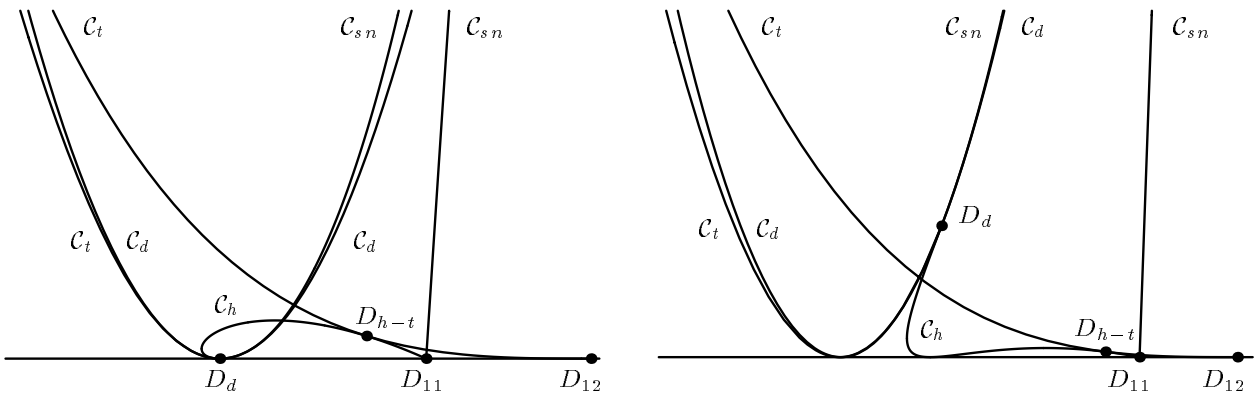


Figure 8: